Autophagosomes cooperate in the degradation of intracellular C-terminal fragments of the amyloid precursor protein via the MVB/lysosomal pathway

González, Alexis E.; Muñoz, Vanessa C.; Cavieres, Viviana A.; Bustamante, Hianara A.; Cornejo, Víctor-Hugo; Januário, Yunan C.

Published in:
FASEB Journal

DOI:
10.1096/fj.201600713R

Publication date:
2017

Document Version
Peer reviewed version

Autophagosomes cooperate in the degradation of intracellular C-terminal fragments of the Amyloid Precursor Protein via the MVB/lysosomal pathway

Alexis E. González[1], Vanessa C. Muñoz[1], Viviana A. Cavieres[1], Hianara A. Bustamante[1], Víctor-Hugo Cornejo[2], Yunan C. Januário[3], Ibeth González[1], Claudio Hetz[2], Luis L. daSilva[3], Alejandro Rojas-Fernández[4,5], Ronald T. Hay[4] Gonzalo A. Mardones[1,5], and Patricia V. Burgos[1,5,*]

[1]Department of Physiology, School of Medicine, Universidad Austral de Chile, Valdivia 5110566, Chile

[2]Biomedical Neuroscience Institute, Faculty of Medicine, University of Chile, Santiago 8380453, Chile

[3]Department of Cell and Molecular Biology, Ribeirão Preto Medical School, University of São Paulo, Ribeirão Preto, Brazil

[4]Centre for Gene Regulation and Expression, College of Life Sciences, University of Dundee, Dow Street, Dundee, DD1 5EH, Scotland, United Kingdom

and

[5]Center for Interdisciplinary Studies of the Nervous System (CISNe), Universidad Austral de Chile, Valdivia 5110566, Chile

* Corresponding author at:

Patricia V. Burgos, Laboratory of Cell & Molecular Biology, Department of Physiology, School of Medicine, Universidad Austral de Chile, Valdivia 5110566, Chile. Phone: 56-63-2293129, Fax: 56-63-2221513, E-mail: patricia.burgos@uach.cl

Short title:

Turnover control of C99 by autophagosomes and MVBs.

Link to final published version DOI: 10.1096/fj.201600713R

ABBREVIATIONS

Aβ, amyloid beta; AD, Alzheimer's disease; AICDγ, APP intracellular domain; APP, β-amyloid precursor protein; C83, carboxy-terminal fragment-α; C99, carboxy-terminal fragment-β; ILVs, intraluminal vesicles; MVBs, multivesicular bodies

ABSTRACT

Brain regions affected by Alzheimer's disease display well-recognized early neuropathological features in the endo-lysosomal and autophagy systems of neurons, including enlargement of endosomal compartments, progressive accumulation of autophagic vacuoles, and lysosomal dysfunction. Although the primary causes of these disturbances are still under investigation, a growing body of evidence suggests that the amyloid precursor protein (APP) intracellular C-terminal fragment-β (C99), generated by cleavage of APP by BACE1, is the primary cause of the endosome enlargement in AD and the earliest initiator of synaptic plasticity and long-term memory impairment. The aim of the present study was to evaluate the possible relationship between the endo-lysosomal degradation pathway and autophagy on the proteolytic processing and turnover of C99. Herein, we show that pharmacological treatments that either inhibit autophagosome formation or block the fusion of autophagosomes to endo-lysosomal compartments caused an increase in C99 levels. We also show that inhibition of autophagosome formation by depletion of Atg5 led to higher levels of C99 and to its massive accumulation in the lumen of enlarged perinuclear, LAMP1-positive organelles. In contrast, activation of autophagosome formation, either by starvation or by inhibition of the mammalian target of rapamycin, enhanced lysosomal clearance of C99. Altogether, our results indicate that autophagosomes are key organelles to help avoid C99 accumulation preventing its deleterious effects.

Keywords:

Alzheimer's disease, APP, autophagosomes, C99, lysosomes, multivesicular bodies.

INTRODUCTION

Alzheimer's disease (AD) is the most common form of dementia. However, the identification of cell biological processes that cause AD remains a challenge. An important feature of brain regions of patients affected by AD is the accumulation of protein aggregates, namely tau tangles and amyloid-β (Aβ) plaques (1, 2). Aβ plaques are formed during the so-called amyloidogenic cleavage of the amyloid precursor protein (APP), which starts with the β-site APP cleaving enzyme 1 (BACE1) that generates a C-terminal fragment (CTF) named C99 (also called CTFβ; Fig. 1A). In contrast, nonamyloidogenic cleavage of APP by α-secretases generates a shorter CTF called C83 (also known as CTFα; Fig. 1A). The transmembrane domain of each CTF is further cleaved by γ-secretase, which generates additional fragments: Aβ and AICDγ for C99, or p3 and AICDγ for C83 (3, 4) (Fig. 1A).

Although enhancement of amyloidogenic proteolytic processing of APP is considered crucial to AD pathogenesis, several reports indicate that defects in autophagy and the endo-lysosomal pathway of protein degradation are also critical (5-7). Autophagy can proceed via three mechanistically distinct pathways: macroautophagy, microautophagy and chaperone-mediated autophagy (8). Macroautophagy deficiency in mice brain results in neurodegeneration and is characterized by accumulation of ubiquitylated-protein aggregates (9), highlighting the importance of this pathway in neuronal homeostasis. Central to macroautophagy is the existence of transitory organelles called autophagosomes. Formation of autophagosomes occurs constitutively under normal nutrient conditions (9, 10), but is highly inducible by cellular stress such as amino acid starvation and inhibition of the key cell regulator mammalian target of rapamycin (mTOR) (11). Autophagosomes sequester cytoplasmic constituents and fuse with lysosomes to form autolysosomes, promoting degradation of sequestered content to recycle macromolecules, a process known as autophagy-flux (12). Ultrastructural studies of the brain of post mortem AD patients revealed that autophagic organelles including autophagosomes and autophagolysosomes gradually accumulate in dystrophic neurites, a neuropathological hallmark of AD, having important implications in Aβ peptide generation and neuronal survival in later stages of AD (13, 14). Although these findings explain the lower rates of protein degradation in AD neurons, it is still under study how to manipulate these pathways to increase protein clearance in neurons (15, 16).

Autophagosomes can also fuse to pre-lysosomal endocytic organelles, such as late endosomes, also called multivesicular bodies (MVBs). Fusion of autophagosomes to MVBs generates a hybrid organelle called amphisome, which ultimately also fuses to lysosomes (17, 18). Biogenesis of MVBs involves the formation of intraluminal vesicles (ILVs), which requires the activity of the four, multi-subunit Endosome Sorting Complexes Required for Transport (ESCRTs 0 to III), collectively called the ESCRT machinery

(19, 20). Macroautophagy is abrogated in cells depleted of ESCRT subunits (21, 22), indicating a close interaction between these two pathways (10, 23).

Intracellular trafficking of APP includes its targeting to endo-lysosomal membranes, either from the *trans*-Golgi network (TGN) sorted by the AP-4 adaptor complex (24, 25), or from the plasma membrane by endocytosis (26, 27). Several studies have demonstrated that APP is normally incorporated into the ILVs of MVBs in a process dependent on the ESCRT machinery (26, 28, 29). However, it is still under debate if the MVB pathway prevents amyloidogenic processing of APP (28, 29), or increases Aβ production (26). Moreover, it is not clear how the ESCRT machinery affects both APP processing and CTFs levels, and whether its effects are a consequence of ILV formation or via autophagy-flux (21, 22) (30). Positive regulators of macroautophagy, such as SMER28 (31) and the transcription factor EB (TFEB) (32) reduce the levels of APP and its CTFs. However, the mechanism that explains how autophagosomes impact the turnover of APP and its CTFs remains unknown. In the present study, we show that inhibition of either autophagosome formation or the fusion of autophagosomes with endo-lysosomal compartments caused a dramatic increase in CTFs levels. Surprisingly, microscopy analysis revealed that these CTFs accumulated in structures resembling ILVs of MVBs. In agreement with these findings, we show that activation of autophagosome formation, either by starvation or treatment with the mTOR inhibitor Torin-1, enhanced C99 lysosomal clearance. Therefore, we propose that autophagosomes are key organelles that connect with the MVB/lysosomal pathway for efficient turnover of CTFs.

MATERIAL AND METHODS

Chemical reagents and antibodies

Bafilomycin A1 (BfaA1), Chloroquine (CQ), Earle's balanced salt solution (EBSS), N-[N-(3,5-difluorophenacetyl)-L-alanyl]-S-phenylglycine *t*-butyl ester (DAPT), puromycin dihydrochloride, thapsigargin, and a cocktail of protease inhibitors were purchased from Sigma-Aldrich. Torin-1 was purchased from TOCRIS. The selective Vps34 inhibitor Vps34-IN1 was purchased from MedKoo Biosciences. We used the following mouse monoclonal antibodies: clone C4 anti-β-Actin, clone 51 anti-TSG101 and clone 3 anti-p62 (BD Biosciences); clone WO2 anti-C99 fragment (Merck Millipore); clone H4A3 anti-LAMP1, clone H4B4 anti-LAMP2 and clone H5C6 anti-CD63 (Developmental Studies Hybridoma Bank); and anti-GFP (Roche Applied Science). We used the following polyclonal antibodies: human anti-EEA1 (kindly provided by A. González, Pontificia Universidad Católica, Chile); rabbit anti-Cathepsin D (R&D Systems); rabbit anti-LC3 and rabbit anti-Atg5 (Cell Signaling Technology); and rabbit anti-APP (Invitrogen). HRP-conjugated secondary antibodies were purchased from Jackson ImmunoResearch, and 4',6-diamidino-2-phenylindole (DAPI) and fluorophore-conjugated secondary antibodies were from Life Technologies.

Cell culture, plasmids and generation of stable cell lines

H4 human neuroglioma cells were obtained from the American Type Culture Collection. H4-derived cell lines were cultured in Dulbecco's modified Eagle's medium (DMEM), supplemented with 10% heat-inactivated fetal bovine serum (FBS) and penicillin/streptomycin (Life Technologies), in a 5% CO_2 atmosphere at 37°C. The generation of H4 stable cell lines expressing either HA-tagged APP_{695}-F/P-D/A-EGFP (APP-GFP) or C99-F/P-D/A-EGFP (C99-GFP) was previously reported (33). Stably transfected cells were maintained in culture medium supplemented with 100 μg/ml G418. Cells were grown to subconfluence, and treated with drugs or lentiviral particles containing specific shRNAs for further western blot and immunofluorescence analysis. Nutrient starvation assays were performed in the presence of EBSS.

RNA interference (RNAi) with siRNA

A small interfering RNA (siRNA) designed to target human TSG101 (5'-CCU CCA GUC UUC UCU CGU C-3') was purchased from Dharmacon (Lafayette, CO). siRNA transfections were carried out using the Oligofectamine reagent from Invitrogen (Camarillo, CA, USA), using similar conditions as described previously (25).

RNA interference (RNAi) with shRNA

We generated stable H4 neuroglioma cell lines with reduced Atg5 levels by introducing shRNA-containing lentiviral particles. shRNA sequences were cloned in the pLKO.1 vector, and a shRNA against the luciferase gene was used as a control. Lentiviral particles were generated by co-transfection of HEK293 cells with pLKO.1-shRNA constructs (1 μg), VSV-g (1 μg) and pΔ8.9 (1 μg). Transfection was performed with Lipofectamine 2000 (Invitrogen) following the manufacture's instructions. Forty-eight hours post-transfection, the medium containing lentiviral particles was transferred to H4 cells at a 1:2 dilution in the presence of 8 μg/ml polybreen. After 24-h, cells were selected with 3 μg/ml of puromycin. pLKO.1 vectors were generated by The Broad Institute (Boston, MA; http://www.broad.mit.edu/genome_bio/trc/rnai.html). Stable H4 cells with reduced Atg5 levels were maintained in medium containing 3 μg/ml puromycin. We used a shRNA sequence against Atg5 that we selected and described previously (34).

Preparation of protein extracts and western blotting

Cells were washed in cold PBS and lysed at 4°C in lysis buffer (50 mM Tris-HCl pH 7.4, 150 mM NaCl, 1 mM EDTA, 1% Triton X-100) supplemented with a cocktail of protease inhibitors (Sigma-Aldrich). Lysates were cleared by centrifugation at 16,000 *g* for 20 min at 4°C, and protein concentration was determined with a protein assay solution (Bio-Rad Laboratories, Hercules, CA, USA). Samples with equivalent amount of protein were boiled for 5 min with Laemmli SDS-PAGE sample buffer, and analyzed by SDS-PAGE. Proteins were

electroblotted onto nitrocellulose membranes and incubated sequentially with primary and secondary antibodies for 1 h at room temperature, or overnight at 4ºC. Chemiluminescence protein detection was performed using Pierce Western Blotting Substrate (Thermo Scientific). β-actin was used as an internal loading control.

Fluorescence microscopy

Cells grown on glass coverslips were washed with PBS and fixed with 4% paraformaldehyde for 30 min at room temperature (RT). After fixation, cells were washed with PBS and permeabilized with 0.2% Triton X-100 in PBS for 10 min at RT. Cells were incubated with the indicated primary antibodies diluted in immunofluorescence buffer (PBS containing 10% fetal bovine serum and 0.1% (w/v) saponin) for 45 min at 37ºC. Coverslips were PBS-washed and incubated with the corresponding fluorophore-conjugated secondary antibody diluted in immunofluorescence buffer, for 30 min at 37ºC. For nuclei staining, cells were PBS-washed and incubated for 10 min at RT with 0.1 μg/ml DAPI. After the final wash, coverslips were mounted onto glass slides with Fluoromount-G (SouthernBiotech). Images of fixed cells were acquired with an AxioObserver.D1 microscope equipped with a PlanApo 63× oil immersion objective (NA 1.4) and an AxioCam MRm digital camera (Carl Zeiss), using similar settings described previously (34), or with an Olympus FluoView FV1000 scanning unit fitted on an inverted Olympus IX81 microscope equipped with a PlanApo 60× oil immersion objective (NA 1.4; Olympus), using similar settings as described previously (35). Alternatively, images of fixed cells were acquired by a DeltaVision OMX system for super-resolution by structured illumination microscopy, using similar settings as described previously (36) (37). For fluorescent signal quantification, 12-bit or 16-bit images (Z-stack, with 0.2 μm intervals) were acquired under identical settings avoiding signal saturation, and each image was corrected for the background. The corrected fluorescent signal in each cell of each image was used to determine the total integrated pixel intensity per cell area using Image J software 1.44o (Wayne Rasband, NIH, http://imagej.nih.gov). Colocalization analyses and estimation of the Pearson's correlation coefficient (38) were performed as described (35).

Densitometric quantification and statistical analysis

Quantification of immunoblot signals was performed using Image J software 1.44o. For each condition, protein bands were quantified from at least three independent experiments. Data analysis was performed using Microsoft Excel 2011 (Microsoft Corporation) or Prism 5.0 (GraphPad Software). Results were represented in graphs depicting the mean ± standard deviation. Statistical significance was determined by two-tailed, paired *t*-test. *P*-values > 0.05 or ≤ 0.05 were regarded as not statistically significant or statistically significant, respectively. In the figures, *P*-values between 0.01 and 0.05 are indicated with one asterisk, *P*-values between 0.001 and 0.01 are indicated with two asterisks and *P*-values less than 0.001 are indicated with three asterisks.

RESULTS

Impaired lysosomal activity increases APP full-length and C99 levels

Previous reports have demonstrated that the perturbation of lysosomal pH causes an increase in the levels of APP and CTFs (33, 39). However, it is not well defined if all CTFs fragments are equally perturbed by lysosomal dysfunction. Herein, we used a H4 human neuroglioma cell line stably expressing a GFP-tagged amyloidogenic version of APP (APP-GFP), which we previously used to facilitate the detection of C99 in the form of C99-GFP (33, 40). We tested the effect of chloroquine (CQ) and bafilomycin A1 (BfaA1) on the levels of APP-GFP, C99-GFP and C83-GFP (Fig. 1A). CQ and BfaA1 are two drugs that raise organelle pH in the late secretory pathway, resulting in perturbation of both endosomal maturation and lysosomal function (41). Western blot analysis showed that treatment with CQ or BfaA1 led to a significant ~2.4-fold or ~2.1-fold increase in APP levels, respectively, compared to non-treated cells (Fig. 1B, lanes 1, 3 and 5, and Fig. 1C). To detect C99-GFP and C83-GFP, we treated cells with DAPT, a specific γ-secretase inhibitor (42). As expected, western blot analysis using the WO2 antibody (that distinguishes between C99 and C83; Fig. 1A) (43) showed that incubation with DAPT alone caused a steady state accumulation of C99-GFP (Fig. 1B, lanes 1 and 2). We observed that in the presence of DAPT the treatment with CQ caused a significant ~1.8-fold increase in C99-GFP levels, compared to cells treated with DAPT alone (Fig. 1B, lanes 2 and 4, and Fig. 1C). Likewise, treatment with BfaA1 in the presence of DAPT caused a significant ~3.0-fold increase in C99-GFP levels (Fig. 1B, lanes 2 and 6, and Fig. 1C). In contrast, we found that in the presence of DAPT the treatment with CQ or BfaA1 led to a significant decrease of C83-GFP to ~55% or ~45%, respectively, of the levels found in control cells (Fig. 1B, lanes 2, 4 and 6, and Fig. 1C). In addition, we found that a combination of BfaA1, E64 and leupeptin, a cocktail that strongly perturbs lysosomal function (44), increased the levels of endogenous C99 (Fig. S1). Together, these results indicate that impaired lysosomal function causes a differential effect on the CTFs, suggesting that C99 could be a better substrate of lysosomes.

Depletion of TSG101 increases the levels of APP, CTFs, and the number of autophagosomes

Several studies propose that APP is normally sorted into ILVs of MVBs, and that this process is dependent on the ESCRT machinery (26, 28, 29). Although these studies demonstrated that depletion of the ESCRT-0 subunit HRS, or of the ESCRT-I subunit TSG101, block APP sorting into ILVs, it is still a matter of discussion if these disturbances promote amyloidogenic processing (28, 29), or reduce Aβ production (26). Therefore, we evaluated whether the formation of MVBs was important for lysosomal degradation of C99. For this, we investigated the effect of depleting TSG101 by RNAi in H4 cells expressing the amyloidogenic version of APP-GFP. Western blot analysis showed that siRNA-mediated depletion of TSG101 led to a significant increase in APP-GFP levels, compared to a non-targeting siRNA (siNT), detected both in the absence or presence of DAPT (Fig. 2, A and B). As expected, DAPT caused a steady state accumulation of both C99-GFP and C83-GFP in

cells transfected with siNT (Fig. 2A, lanes 1 and 2). In the presence of DAPT, we detected that TSG101 depletion caused a significant increase in the levels of C99-GFP and C83-GFP compared to control cells (Fig. 2A, lanes 2 and 4, and Fig. 2B). This result suggests that the degradation of CTFs is greatly enhanced when the MVB pathway is functioning normally.

To study whether the depletion of TSG101 affected APP-GFP or CTFs localization, we performed a confocal microscopy analysis. In different cell types, including H4 cells, a large proportion of the steady-state distribution of endogenous APP is in early endosomes (26, 45). Similarly, in H4 cells the majority of APP-GFP localizes in early endosomes (25). Consistent with this notion, we found that in cells transfected with siNT little APP-GFP colocalized with LAMP1, a late endosome/MVB/lysosome protein (Fig. S2, A-C and G-H). In contrast, depletion of TSG101 resulted in a significant redistribution of APP to enlarged, LAMP1-containing endo-lysosomal compartments (Fig. S2, D-H). We obtained similar results with RNAi-mediated depletion of HRS (data not shown). Together, these findings suggested that impaired MVB formation caused accumulation of APP and CTFs in altered endo-lysosomal compartments.

Because MVBs eventually fuse with autophagosomes (17), we hypothesized that increased levels of APP and CTFs in TSG101 depleted cells could be the result of autophagosome accumulation. Therefore, we analyzed by confocal fluorescence microscopy the presence of puncta containing the protein p62. During autophagy, these puncta recruit specific ubiquitylated cargos by binding to the ubiquitin-associated (UBA) domain of p62 (46), puncta that accumulate when the fusion of autophagosomes with endo-lysosomal compartments is blocked (47). We found that H4 cells depleted of TSG101 showed a significant increase in the number of puncta containing p62, compared to cells treated with siNT (Fig. S3, A, D, and G), in agreement with the effect of a similar treatment in HeLa cells (22). A classical marker of autophagosomes is the protein LC3 (47), and accordingly we found a significant colocalization of p62-containing puncta with LC3 (Fig. S3, D-F, and N), compared to the negligible colocalization of p62-containing puncta with the lysosomal protein Cathepsin D (Fig. S3, K-N). These results indicate that TSG101 depletion precludes autophagy-flux and hence this effect could be the cause of APP-GFP and CTFs accumulation. To further analyze whether the accumulation of APP-GFP and the CTFs is produced when autophagosomes are accumulated, we studied the effect of thapsigargin, a drug that inhibits the fusion of autophagosomes to lysosomes (48). As expected, we found that cells treated with thapsigargin also accumulated p62-containing puncta (Fig. S4, A and E), similar to the effect reported for MEFs cells (48). Moreover, we observed a significant higher colocalization of the p62-containing puncta with LC3, compared to that with Cathepsin D (Fig. S4, A-J), indicating that thapsigargin is also a potent inhibitor of autophagy-flux in H4 cells. Western blot analysis showed that thapsigargin caused a significant increase in the levels of both APP-GFP and C99-GFP, but with no apparent effect in the levels of C83-GFP (Fig. S4, K and L), suggesting that the

disruption of autophagy-flux by thapsigargin affects differentially the turnover of APP species. Nevertheless, because the treatment with thapsigargin can also result in stress of the endoplasmic reticulum (ER) (49), we also analyzed the effect of the treatment with Vps34-IN1, which is a selective inhibitor of Vps34, a class III phosphatidylinositol 3-kinase that is required for autophagosome formation (50, 51). As expected, immunofluorescence analysis showed both that nutrient starvation by incubating cells in EBSS resulted in accumulation of puncta that contained LC3 and p62 (Fig. 3, A-F), and that the treatment with Vps34-IN1 of cells incubated in complete medium did not accumulate puncta containing LC3 or p62 (Fig. 3, G-I). In contrast, the treatment with Vps34-IN1 of cells incubated in EBSS reduced significantly the accumulation of puncta containing LC3 and p62 (Fig. 3, J-M), confirming that Vps34-IN1 is a potent blocker of autophagosome biogenesis (52). Additional confirmation of the effect of Vps34-IN1 was obtained by western blot analysis that showed a time-dependent increase in the levels of LC3-I, and a corresponding decrease in the levels of LC3-II, which is the lipidated form of LC3 that decorates autophagosomes (53) (Fig. 3N). Interestingly, the treatment with Vps34-IN1 caused a time-dependent increase in the levels of endogenous C99, although with no apparent effect on the levels of endogenous APP or C83 (Fig. 3N). Altogether, our results indicate that different treatments that disrupt autophagy lead to C99 accumulation.

Depletion of Atg5 accumulates endogenous CTFs in the lumen of enlarged MVBs

Atg5 conjugated to Atg12 is part of a protein complex that also contains Atg16L, a complex that controls an essential step in autophagosome formation (54). Therefore, to further study the contribution of autophagosomes in the clearance of APP/CTFs, we analyzed by western blot the steady-state levels of endogenous APP and CTFs in H4 cells stably depleted of Atg5 by shRNA-mediated RNAi. We found that cells stably expressing a shRNA targeting Atg5 (shAtg5) the levels of APP were significantly decreased to ~50% the levels found in cells expressing a control shRNA (shLuc; Fig. 4A, lanes 1 and 3, and Fig. 4B). We observed a similar result in cells treated with DAPT (Fig. 4A, lanes 2 and 4, and Fig. 4C), indicating that decreased APP levels were not the result of increased γ-secretase activity. Moreover, we found that in contrast to control cells, the levels of APP in Atg5 depleted cells were not rescued with the combination of BfaA1, E64 and leupeptin (Fig. S5), indicating that the decreased level of APP in Atg5 depleted cells was not the result of an increase in APP degradation. On the other hand, we observed a significant ~3.9-fold increase in C99 levels in Atg5 depleted cells (Fig. 4A, lanes 1 and 3, and Fig. 4B). We also observed a significant ~23.1-fold increase in C83 levels in Atg5 depleted cells (Fig. 4A, lanes 1 and 3, and Fig. 4B). These observations strongly indicate that perturbation of Atg5-dependent autophagy results in augmented proteolytic processing of APP, with generation of CTFs that ultimately accumulate.

To evaluate the possible effect of the γ-secretase activity on the levels of CTFs in Atg5 depleted cells we treated cells with DAPT. Treatment of control cells with DAPT resulted in increased levels of both, C99 and C83 (Fig.

4A, lanes 1 and 2), indicative of the expected γ-secretase activity on the CTFs. In Atg5 depleted cells treatment with DAPT also resulted in a significant increase in the levels of both CTFs (Fig. 4A, lanes 3 and 4, and Fig. 4C). However, when comparing the treatment with DAPT between control and Atg5-depleted cells we observed that the levels of C99 underwent the most significant increase: ~7.9-fold increase of C99 versus ~2.0-fold increase of C83 (Fig. 4A, lanes 2 and 4, and Fig. 4D). These results are consistent with the notion that impaired autophagosome formation caused increased amylodogenic processing of APP.

To determine the effect that Atg5 depletion could have on the intracellular localization of APP and CTFs, we performed immunofluorescence analysis using an antibody targeting the C-terminal, cytosolic domain of APP (anti-Tail; Fig. 1A), and examined cells by confocal microscopy. Consistent with the localization of APP-GFP, we found that in control H4 cells little endogenous APP/CTFs localized in MVBs/lysosomes decorated with antibody to LAMP1, and that a higher proportion localized instead in early endosomes decorated with antibody to EEA1 (Fig. 5, A-D, and I-L). In contrast, Atg5 depletion led to a significant ~3.0-fold increase in the colocalization of APP/CTFs with LAMP1, and a corresponding significant decrease in the colocalization with EEA1 to ~45% the levels found in control cells (Fig. 5, E-H, and I-L). Similarly, we observed that depletion of Atg5 led to a significant ~2.6-fold increase in APP/CTFs colocalization with Cathepsin D, while the expected colocalization of Cathepsin D with LAMP1 remained largely unaffected (Fig. S6, B-C, F-G, K and M). On the other hand, quantification of fluorescence intensity showed a significant ~4.6-fold increase in the levels of APP/CTFs in Atg5 depleted cells (Fig. 5M). This last result correlates with the western blot analysis (Fig. 4A), and further supports the conclusion that Atg5 depletion causes a massive increase in APP/CTFs levels in organelles positive to LAMP1 and Cathepsin D. Because the anti-Tail antibody recognizes the cytosolic domain of APP and both CTFs, the APP species that accounts for the increase in fluorescence intensity cannot be discriminated. Nevertheless, the western blot analysis suggests that the majority of the fluorescence signal corresponded to CTFs. We also observed that in cells depleted of Atg5 the organelles decorated with antibodies to LAMP1 or Cathepsin D were enlarged, and were mainly localized at the perinuclear region (Fig. 5, B and F, and Fig. S6, B and F), in agreement with a previous study performed in mouse embryonic fibroblasts (55), suggesting that depletion of Atg5 caused a disruption of MVBs/lysosomes. Accordingly, these Cathepsin D and LAMP1-positive large organelles were also positive to CD63 (Fig S7, A-F) and to LAMP2 (Fig. S7, G-L), both proteins also localized mainly in MVBs/lysosomes (56, 57), and that similar to the colocalization of Cathepsin D with LAMP1, the colocalization of Cathepsin D with CD63 or LAMP2 was unaffected in cells depleted of Atg5 (Fig S7, M and N). All these results strongly suggest that Atg5 depletion perturbs the homeostasis of MVBs/lysosomes, condition that enhances the accumulation of intracellular CTFs.

To analyze in more detail the organelles that accumulate CTFs in Atg5 depleted cells we used super resolution, structured illumination microscopy (SIM). As shown by standard confocal microscopy (Fig. 5, A-C), most of

the APP/CTFs fluorescent signal in control cells was detected in cytoplasmic structures that were different to MVBs/lysosomes decorated with antibody to LAMP1 (Fig. 6, A-C). However, the APP/CTFs fluorescent signal in Atg5 depleted cells was detected in structures resembling ILVs of enlarged LAMP1-containing MVBs (Fig. 6, D-G). Moreover, fluorescence intensity analysis of SIM images showed that the APP/CTFs signal is restricted to the lumen of enlarged LAMP1-containing organelles and therefore excluded from their limiting membrane, suggesting that APP/CTFs were efficiently sorted into ILVs (Fig. 6, G-H). These results indicate that accumulation of APP/CTFs in Atg5 depleted cells was not due to impaired incorporation of APP/CTFs into ILVs. Together, this suggests that APP/CTFs are sorted into ILVs of MVBs en route to lysosomes for degradation.

Activation of autophagy promotes intracellular clearance of C99

Our results showed that autophagosomes are necessary for the clearance of intracellular CTFs via the endo-lysosomal pathway. To directly examine the active role of autophagy in C99 clearence, we subjected H4 cells stably expressing C99-GFP to nutrient starvation by incubation in EBSS, an established treatment that activates autophagy (16). Western blot analysis showed that nutrient starvation led to a significant, time-dependent reduction in C99-GFP levels, as well as of AICDγ-GFP (Fig. 7, A and B). Likewise, treatment with Torin-1, a potent and selective inhibitor of mTORC1/2 that also activates macroautophagy (58), similarly reduced C99-GFP and AICDγ-GFP levels in a time-dependent manner (Fig. 7, C and D). Treatment with either EBSS or Torin-1 in the presence of DAPT did not prevent the reduction of both C99-GFP and AICDγ-GFP levels (Fig. 7, E and F), indicating that the reduction in the levels of C99-GFP was not the result of γ-secretase activity. These last results strongly indicate that autophagy can participate in the clearance of amyloidogenic APP fragments. All the results shown in the present report are consistent with a model of a concerted function of autophagosomes and the MVB pathway for the clearance of amyloidogenic C99.

DISCUSSION

Several lines of evidence indicate that defects in long-term potentiation and cognitive impairment correlate better with increased intracellular Aβ-like immunoreactivity than with the presence of extracellular Aβ aggregates (59-61). The analysis of a murine model of AD (3xTgAD mice) showed that intracellular accumulation of early and age-dependent Aβ-like species corresponds to C99 rather than full-length APP or the Aβ peptide (59). Thus, C99 seems to be the earliest initiator of synaptic plasticity and long-term memory impairment in AD (62), presumably due to its early accumulation at the hippocampus (59, 61).

Although the cause of C99 accumulation remains unknown, several early studies point-out abnormalities of endo-lysosomal compartments within neurons located in affected brain regions of patients with AD (7, 14). The abnormalities include an increased number of endo-lysosomal compartments, particularly in the cell soma of pyramidal neurons (7). Of note, the dependence of neuronal function on the endo-lysosomal system is well documented because of the existence of many lysosomal primary disorders, in which defects in lysosomal function cause severe neurodegeneration phenotypes (63), including pathological features of AD (64).

Early accumulation of C99 in enlarged endo-lysosomal neuronal compartments of 3xTgAD mice suggests an impaired clearance of C99 by the endo-lysosomal system (59). In fact, it has been proposed that depletion of some ESCRT subunits inhibits APP sorting into ILVs of MVBs (26, 28, 29). In agreement with this, we found that TSG101 depletion in H4 cells caused an increase in APP-GFP levels detected by western blot analysis, which correlated with accumulation of APP-GFP in enlarged endo-lysosomal compartments decorated with antibodies to LAMP1. Moreover, we found that TSG101 depletion increased CTFs levels, suggesting that CTFs are also sorted into ILVs. We also observed a robust increase in the levels of C99-GFP and endogenous C99 in response to treatments that perturb lysosomal function, supporting the conclusion that lysosomes are implicated in C99 clearance, as well as in APP turnover (26, 33, 61). Moreover, perturbed lysosomal function led to a significant decrease in C83-GFP levels. These results indicate that proper lysosomal function favor the non-amyloidogenic processing of APP preventing the accumulation of C99. Interestingly, TSG101 depletion results in accumulation of APP/CTFs in an endo-lysosomal compartment that appears to contain proteins of both early endosomes and MVBs/lysosomes, such as EEA1 and LAMP1, respectively (26, 28, and the present study), emphasizing the need of normal maturation of early endosomes into MVBs to avoid accumulation of amyloidogenic proteins.

In addition to the evidence showing that APP is sorted to the endo-lysosomal pathway for delivery to lysosomes (25, 26, 28, 33), other findings indicate that the cellular levels of both APP and C99 are also regulated by autophagy (31, 32, 34). However, the contribution of both pathways in the total clearance of these amyloidogenic membrane proteins remains unknown. In this regard, different reports indicate that the endo-lysosomal system is functionally connected to autophagy (10, 17, 18, 23). In fact, autophagosomes can fuse to MVBs prior to lysosome delivery (18). Moreover, depletion of some ESCRT subunits accumulates autophagosomes by precluding their fusion to MVBs or lysosomes (22, 30, 65). In the present study, we show that, similar to HeLa cells (22), TSG101 depletion in H4 cells also inhibited autophagy-flux. We found that TSG101 depletion resulted in accumulation of APP species in endo-lysosomal organelles containing LAMP1. To distinguish between autophagy-flux inhibition and impaired sorting into ILVs of MVBs as the cause of APP and CTFs accumulation in TSG101 depleted cells, we investigated the effect of treatment with thapsigargin.

Thapsigargin is a classical stressor of the ER (66) that also blocks the fusion of autophagosomes to endo-lysosomal compartments, but by hampering recruitment of Rab7 to autophagosomes, a critical step during macroautophagy (48). Treatment with thapsigargin resulted in impaired autophagy-flux and increased APP and C99 levels, which is consistent with the notion that autophagy is critical for APP/CTFs clearance. In addition, we found increased levels of endogenous C99 upon selective inhibition of Vps34, which is a kinase that produces phosphatidylinositol-3-phosphate (PI3P), a crucial lipid for autophagosome nucleation and maturation (50, 51). This result is in agreement with a previous report showing that silencing of Vps34 enhances the production of Aβ in primary mouse cortical neurons (29). Because inhibition of Vps34 also resulted in inhibition of both basal autophagy and autophagy induced by nutrient starvation, the higher levels of Aβ peptide in cells depleted of Vps34 could be consequence of impairment in the MVB/lysosomal pathway due to perturbed autophagosome biogenesis. Together, these results suggest that autophagosomes are necessary for the degradation of C99 in the MVB/lysosomal pathway. Thus, increased CTFs levels in LAMP1-containing organelles during impaired, basal Atg5-dependent autophagy provide additional support to the notion that autophagy-flux is necessary for C99 clearance. Moreover, our SIM analysis in Atg5 depleted cells strongly suggests that accumulation occurred in ILVs of enlarged MVBs.

Because the fusion between an autophagosome and an MVB is the convergence point between these two pathways (17, 18), our findings indicate that upon Atg5-dependent autophagy-impairment the MVB/lysosomal pathway could be dramatically affected, and hence the degradation of cargos such as APP/CTFs. In this regard, we showed that Atg5 depletion caused an apparent accumulation of CTFs in perinuclear, enlarged organelles positive to LAMP1, as well as positive to CD63, LAMP2 and Cathepsin D, suggesting that a dramatic effect on the maturation of MVBs affected the degradation of CTFs. In contrast, recent studies in murine models of Down syndrome and Alzheimer's disease show that C99 accumulates in enlarged early endosomes that contain over activated Rab5 (67-69), suggesting the intriguing possibility that in those cases a similar mechanism of inter organelle fusion is impaired, although is not well known whether or not autophagosomes can fuse to early endosomes (70, 71). Nevertheless, our immunofluorescence analysis to EEA1 showed no apparent differences in the morphology of early endosomes in control and Atg5 depleted cells. In addition, we observed a reduction in the colocalization of APP/CTFs and EEA1 upon Atg5 depletion, suggesting that perturbations at different levels of the endo-lysosomal system could lead to a similar outcome of C99 accumulation. Likewise, it will be important to determine if an initial accumulation of C99 triggers the enlargement of endo-lysosomal organelles affecting their functions. In any case, our results provide strong evidence that autophagosomes cooperate in maintaining reduced levels of C99 either indirectly, by avoiding C99 production in MVBs, or directly, by accelerating C99 degradation in autolysosomes.

Our findings suggested that Atg5 depletion also elicited processing of APP into both C99 and C83. A likely explanation is that APP being accumulated in enlarged MVBs was subsequently processed by α-secretases and/or BACE-1. This is in agreement with the popular idea that amyloidogenic processing of APP occurs mainly in endosomes (72). A different scenario is that APP could have been processed in a pre-endo-lysosomal compartment, such as the ER or the Golgi apparatus, and that the resulting products C83 and C99 accumulated in MVBs. Although less popular, the possibility of amyloidogenic processing in a pre-endosomal compartment is supported by several reports (25, 73). However, the finding that Atg5 depleted cells presented a disproportionate increase of C83 indicates that macroautophagy also plays an important but unexpected role in the nonamylodogenic processing of APP.

Our data allow us to propose that autophagosomes have an important function in APP and CTFs proteostasis. Our proposal is consistent with the observation that autophagosomes gradually accumulate in dystrophic neurites; a well-documented neuropathological hallmark of AD (14). Autophagy has been proposed as an essential activity for neuronal survival, acting as a neuroprotective process activated to alleviate cellular stress (9). In the nervous system a major negative regulator of autophagy is the serine/threonine kinase mTOR, therefore it is plausible that its inhibition would reduce the burden caused by deleterious accumulation of intracellular materials. In support of this notion is the observation that reduced mTOR signaling extends the lifespan of model organisms and protects them against age-related pathologies, including AD (74, 75). Our finding that autophagy activation by two conditions that inhibit mTOR signaling, namely by nutrient starvation or treatment with Torin-1, reduced the levels of C99 highlights this pathway's potential as a pharmacological target.

Collectively, our data support a model in which autophagosomes cooperate in the turnover of C99, as well as of APP and C83, forming an amphisome-like compartment by fusing with MVBs prior to fusion with lysosomes (Fig. 8). Our model predicts that conditions that compromise the fusion of autophagosomes to endo-lysosomal compartments accumulate C99, and thus promote neuronal dysfunction. Further studies will help to clarify whether fusion of autophagosomes with MVBs is a frequent process or a specific event, taking place with a distinct pool of MVBs, and for the clearance of certain cargos, such as APP and CTFs. As a corollary, failures in macroautophagy could impact the balance of proteins that are incorporated into ILVs of MVBs, and therefore we propose that the fate of autophagosomes constitutes an inherent part of the membrane flux that exists in the endo-lysosomal pathway of protein clearance. Hence, the pharmacological booster of autophagy could promote the degradation of C99 and likely of other substrates destined to the endo-lysosomal pathway, emerging as an attractive approach for therapeutic intervention of AD, and eventually of other neurodegenerative disorders related to protein accumulation.

AUTHOR CONTRIBUTIONS

Conceived and designed the experiments: AEG VAC HAB PVB. Performed the experiments: AEG VCM VAC HAB VHC YCJ IC. Analyzed the data: AEG VCM LLD ARF GAM PVB. Contributed reagents/materials/analysis tools: CH LLD RTH GAM PVB. Wrote the paper: AEG GAM PVB.

ACKNOWLEDGEMENTS

This work was funded by grants FONDECYT 1130929 to P.V.B., FONDECYT 1130710 to G.A.M., ECOS/CONICYT C14B03 to P.V.B., Newton-Picarte CONICYT DPI20140068 to P.V.B., DID-UACh D-2013-07 to A.E.G., DID-UACh D-2015-02 to H.A.B., and Programa MECE Educación Superior (UACh). A.E.G., V.A.C., and H.A.B. were supported by fellowships 21110746, 21152294 and 21130315, respectively, from CONICYT. Y.C.J. was supported by a CAPES fellowship from the Brazilian Ministry of Education. The use of the OMX microscope was funded by an MRC Next Generation Optical Microscopy Award (MR/K015869/1).

REFERENCES

1. Masters, C. L., Simms, G., Weinman, N. A., Multhaup, G., McDonald, B. L., and Beyreuther, K. (1985) Amyloid plaque core protein in Alzheimer disease and Down syndrome. *Proc Natl Acad Sci U S A* **82**, 4245-4249
2. Ihara, Y., Nukina, N., Miura, R., and Ogawara, M. (1986) Phosphorylated tau protein is integrated into paired helical filaments in Alzheimer's disease. *J Biochem* **99**, 1807-1810
3. Vassar, R., Kovacs, D. M., Yan, R., and Wong, P. C. (2009) The beta-secretase enzyme BACE in health and Alzheimer's disease: regulation, cell biology, function, and therapeutic potential. *J Neurosci* **29**, 12787-12794
4. De Strooper, B., and Annaert, W. (2010) Novel research horizons for presenilins and gamma-secretases in cell biology and disease. *Annual review of cell and developmental biology* **26**, 235-260
5. Wolfe, D. M., Lee, J. H., Kumar, A., Lee, S., Orenstein, S. J., and Nixon, R. A. (2013) Autophagy failure in Alzheimer's disease and the role of defective lysosomal acidification. *Eur J Neurosci* **37**, 1949-1961
6. Nixon, R. A., and Yang, D. S. (2011) Autophagy failure in Alzheimer's disease--locating the primary defect. *Neurobiol Dis* **43**, 38-45
7. Cataldo, A. M., Hamilton, D. J., Barnett, J. L., Paskevich, P. A., and Nixon, R. A. (1996) Properties of the endosomal-lysosomal system in the human central nervous system: disturbances mark most neurons in populations at risk to degenerate in Alzheimer's disease. *J Neurosci* **16**, 186-199
8. Boya, P., Reggiori, F., and Codogno, P. (2013) Emerging regulation and functions of autophagy. *Nat Cell Biol* **15**, 713-720
9. Hara, T., Nakamura, K., Matsui, M., Yamamoto, A., Nakahara, Y., Suzuki-Migishima, R., Yokoyama, M., Mishima, K., Saito, I., Okano, H., and Mizushima, N. (2006) Suppression of basal autophagy in neural cells causes neurodegenerative disease in mice. *Nature* **441**, 885-889
10. Murrow, L., Malhotra, R., and Debnath, J. (2015) ATG12-ATG3 interacts with Alix to promote basal autophagic flux and late endosome function. *Nat Cell Biol* **17**, 300-310
11. He, C., and Klionsky, D. J. (2009) Regulation mechanisms and signaling pathways of autophagy. *Annual review of genetics* **43**, 67-93
12. Mizushima, N. (2007) Autophagy: process and function. *Genes Dev* **21**, 2861-2873
13. Nixon, R. A. (2007) Autophagy, amyloidogenesis and Alzheimer disease. *J Cell Sci* **120**, 4081-4091
14. Nixon, R. A., Wegiel, J., Kumar, A., Yu, W. H., Peterhoff, C., Cataldo, A., and Cuervo, A. M. (2005) Extensive involvement of autophagy in Alzheimer disease: an immuno-electron microscopy study. *Journal of neuropathology and experimental neurology* **64**, 113-122
15. Wong, Y. C., and Holzbaur, E. L. (2015) Autophagosome dynamics in neurodegeneration at a glance. *J Cell Sci* **128**, 1259-1267
16. Boland, B., Kumar, A., Lee, S., Platt, F. M., Wegiel, J., Yu, W. H., and Nixon, R. A. (2008) Autophagy induction and autophagosome clearance in neurons: relationship to autophagic pathology in Alzheimer's disease. *J Neurosci* **28**, 6926-6937
17. Fader, C. M., and Colombo, M. I. (2009) Autophagy and multivesicular bodies: two closely related partners. *Cell death and differentiation* **16**, 70-78
18. Yi, J., and Tang, X. M. (1999) The convergent point of the endocytic and autophagic pathways in leydig cells. *Cell research* **9**, 243-253
19. Henne, W. M., Buchkovich, N. J., and Emr, S. D. (2011) The ESCRT pathway. *Dev Cell* **21**, 77-91
20. Hurley, J. H., and Hanson, P. I. (2010) Membrane budding and scission by the ESCRT machinery: it's all in the neck. *Nat Rev Mol Cell Biol* **11**, 556-566
21. Lee, J. A., Beigneux, A., Ahmad, S. T., Young, S. G., and Gao, F. B. (2007) ESCRT-III dysfunction causes autophagosome accumulation and neurodegeneration. *Curr Biol* **17**, 1561-1567
22. Filimonenko, M., Stuffers, S., Raiborg, C., Yamamoto, A., Malerod, L., Fisher, E. M., Isaacs, A., Brech, A., Stenmark, H., and Simonsen, A. (2007) Functional multivesicular bodies are required for autophagic clearance of protein aggregates associated with neurodegenerative disease. *J Cell Biol* **179**, 485-500

23. Lamb, C. A., Dooley, H. C., and Tooze, S. A. (2013) Endocytosis and autophagy: Shared machinery for degradation. *BioEssays : news and reviews in molecular, cellular and developmental biology* **35**, 34-45
24. Toh, W. H., Tan, J. Z., Zulkefli, K. L., Houghton, F. J., and Gleeson, P. A. (2016) Amyloid precursor protein traffics from the Golgi directly to early endosomes in an Arl5b and AP4 dependent pathway. *Traffic*
25. Burgos, P. V., Mardones, G. A., Rojas, A. L., daSilva, L. L., Prabhu, Y., Hurley, J. H., and Bonifacino, J. S. (2010) Sorting of the Alzheimer's disease amyloid precursor protein mediated by the AP-4 complex. *Dev Cell* **18**, 425-436
26. Choy, R. W., Cheng, Z., and Schekman, R. (2012) Amyloid precursor protein (APP) traffics from the cell surface via endosomes for amyloid beta (Abeta) production in the trans-Golgi network. *Proc Natl Acad Sci U S A* **109**, E2077-2082
27. Perez, R. G., Soriano, S., Hayes, J. D., Ostaszewski, B., Xia, W., Selkoe, D. J., Chen, X., Stokin, G. B., and Koo, E. H. (1999) Mutagenesis identifies new signals for beta-amyloid precursor protein endocytosis, turnover, and the generation of secreted fragments, including Abeta42. *J Biol Chem* **274**, 18851-18856
28. Edgar, J. R., Willen, K., Gouras, G. K., and Futter, C. E. (2015) ESCRTs regulate amyloid precursor protein sorting in multivesicular bodies and intracellular amyloid-beta accumulation. *J Cell Sci* **128**, 2520-2528
29. Morel, E., Chamoun, Z., Lasiecka, Z. M., Chan, R. B., Williamson, R. L., Vetanovetz, C., Dall'Armi, C., Simoes, S., Point Du Jour, K. S., McCabe, B. D., Small, S. A., and Di Paolo, G. (2013) Phosphatidylinositol-3-phosphate regulates sorting and processing of amyloid precursor protein through the endosomal system. *Nat Commun* **4**, 2250
30. Rusten, T. E., Vaccari, T., Lindmo, K., Rodahl, L. M., Nezis, I. P., Sem-Jacobsen, C., Wendler, F., Vincent, J. P., Brech, A., Bilder, D., and Stenmark, H. (2007) ESCRTs and Fab1 regulate distinct steps of autophagy. *Curr Biol* **17**, 1817-1825
31. Tian, Y., Bustos, V., Flajolet, M., and Greengard, P. (2011) A small-molecule enhancer of autophagy decreases levels of Abeta and APP-CTF via Atg5-dependent autophagy pathway. *Faseb J* **25**, 1934-1942
32. Xiao, Q., Yan, P., Ma, X., Liu, H., Perez, R., Zhu, A., Gonzales, E., Tripoli, D. L., Czerniewski, L., Ballabio, A., Cirrito, J. R., Diwan, A., and Lee, J. M. (2015) Neuronal-Targeted TFEB Accelerates Lysosomal Degradation of APP, Reducing Abeta Generation and Amyloid Plaque Pathogenesis. *J Neurosci* **35**, 12137-12151
33. Bustamante, H. A., Rivera-Dictter, A., Cavieres, V. A., Munoz, V. C., Gonzalez, A., Lin, Y., Mardones, G. A., and Burgos, P. V. (2013) Turnover of C99 is controlled by a crosstalk between ERAD and ubiquitin-independent lysosomal degradation in human neuroglioma cells. *PLoS One* **8**, e83096
34. Cavieres, V. A., Gonzalez, A., Munoz, V. C., Yefi, C. P., Bustamante, H. A., Barraza, R. R., Tapia-Rojas, C., Otth, C., Barrera, M. J., Gonzalez, C., Mardones, G. A., Inestrosa, N. C., and Burgos, P. V. (2015) Tetrahydrohyperforin Inhibits the Proteolytic Processing of Amyloid Precursor Protein and Enhances Its Degradation by Atg5-Dependent Autophagy. *PLoS One* **10**, e0136313
35. Tenorio, M. J., Ross, B. H., Luchsinger, C., Rivera-Dictter, A., Arriagada, C., Acuna, D., Aguilar, M., Cavieres, V., Burgos, P. V., Ehrenfeld, P., and Mardones, G. A. (2016) Distinct Biochemical Pools of Golgi Phosphoprotein 3 in the Human Breast Cancer Cell Lines MCF7 and MDA-MB-231. *PLoS One* **11**, e0154719
36. Schermelleh, L., Carlton, P. M., Haase, S., Shao, L., Winoto, L., Kner, P., Burke, B., Cardoso, M. C., Agard, D. A., Gustafsson, M. G., Leonhardt, H., and Sedat, J. W. (2008) Subdiffraction multicolor imaging of the nuclear periphery with 3D structured illumination microscopy. *Science* **320**, 1332-1336
37. Hattersley, N., Shen, L., Jaffray, E. G., and Hay, R. T. (2011) The SUMO protease SENP6 is a direct regulator of PML nuclear bodies. *Mol Biol Cell* **22**, 78-90
38. Manders, E. M., Stap, J., Brakenhoff, G. J., van Driel, R., and Aten, J. A. (1992) Dynamics of three-dimensional replication patterns during the S-phase, analysed by double labelling of DNA and confocal microscopy. *J Cell Sci* **103 (Pt 3)**, 857-862

39. Siman, R., Mistretta, S., Durkin, J. T., Savage, M. J., Loh, T., Trusko, S., and Scott, R. W. (1993) Processing of the Beta-Amyloid Precursor - Multiple Proteases Generate and Degrade Potentially Amyloidogenic Fragments. *Journal of Biological Chemistry* **268**, 16602-16609
40. Prabhu, Y., Burgos, P. V., Schindler, C., Farias, G. G., Magadan, J. G., and Bonifacino, J. S. (2012) Adaptor protein 2-mediated endocytosis of the beta-secretase BACE1 is dispensable for amyloid precursor protein processing. *Mol Biol Cell* **23**, 2339-2351
41. Yuyama, K., Yamamoto, N., and Yanagisawa, K. (2006) Chloroquine-induced endocytic pathway abnormalities: Cellular model of GM1 ganglioside-induced Abeta fibrillogenesis in Alzheimer's disease. *FEBS letters* **580**, 6972-6976
42. Lanz, T. A., Himes, C. S., Pallante, G., Adams, L., Yamazaki, S., Amore, B., and Merchant, K. M. (2003) The gamma-secretase inhibitor N-[N-(3,5-difluorophenacetyl)-L-alanyl]-S-phenylglycine t-butyl ester reduces A beta levels in vivo in plasma and cerebrospinal fluid in young (plaque-free) and aged (plaque-bearing) Tg2576 mice. *J Pharmacol Exp Ther* **305**, 864-871
43. Sharples, R. A., Vella, L. J., Nisbet, R. M., Naylor, R., Perez, K., Barnham, K. J., Masters, C. L., and Hill, A. F. (2008) Inhibition of gamma-secretase causes increased secretion of amyloid precursor protein C-terminal fragments in association with exosomes. *Faseb J* **22**, 1469-1478
44. Hetz, C., Thielen, P., Matus, S., Nassif, M., Court, F., Kiffin, R., Martinez, G., Cuervo, A. M., Brown, R. H., and Glimcher, L. H. (2009) XBP-1 deficiency in the nervous system protects against amyotrophic lateral sclerosis by increasing autophagy. *Genes Dev* **23**, 2294-2306
45. Lee, J., Retamal, C., Cuitino, L., Caruano-Yzermans, A., Shin, J. E., van Kerkhof, P., Marzolo, M. P., and Bu, G. (2008) Adaptor protein sorting nexin 17 regulates amyloid precursor protein trafficking and processing in the early endosomes. *J Biol Chem* **283**, 11501-11508
46. Pankiv, S., Clausen, T. H., Lamark, T., Brech, A., Bruun, J. A., Outzen, H., Overvatn, A., Bjorkoy, G., and Johansen, T. (2007) p62/SQSTM1 binds directly to Atg8/LC3 to facilitate degradation of ubiquitinated protein aggregates by autophagy. *J Biol Chem* **282**, 24131-24145
47. Rusten, T. E., and Stenmark, H. (2010) p62, an autophagy hero or culprit? *Nat Cell Biol* **12**, 207-209
48. Ganley, I. G., Wong, P. M., Gammoh, N., and Jiang, X. (2011) Distinct autophagosomal-lysosomal fusion mechanism revealed by thapsigargin-induced autophagy arrest. *Mol Cell* **42**, 731-743
49. Li, J., Ni, M., Lee, B., Barron, E., Hinton, D. R., and Lee, A. S. (2008) The unfolded protein response regulator GRP78/BiP is required for endoplasmic reticulum integrity and stress-induced autophagy in mammalian cells. *Cell death and differentiation* **15**, 1460-1471
50. Axe, E. L., Walker, S. A., Manifava, M., Chandra, P., Roderick, H. L., Habermann, A., Griffiths, G., and Ktistakis, N. T. (2008) Autophagosome formation from membrane compartments enriched in phosphatidylinositol 3-phosphate and dynamically connected to the endoplasmic reticulum. *Journal of Cell Biology* **182**, 685-701
51. Jaber, N., Dou, Z. X., Chen, J. S., Catanzaro, J., Jiang, Y. P., Ballou, L. M., Selinger, E., Ouyang, X. S., Lin, R. Z., Zhang, J. H., and Zong, W. X. (2012) Class III PI3K Vps34 plays an essential role in autophagy and in heart and liver function. *P Natl Acad Sci USA* **109**, 2003-2008
52. Bago, R., Sommer, E., Malik, N., Munson, M. J., Prescott, A. R., Davies, P., Natalia, S., Ganley, I. G., and Alessi, D. R. (2015) Characterization of VPS34-IN1, a specific inhibitor of Vps34 reveals that the phosphatidylinositol 3-phosphate binding SGK3 protein kinase is regulated by class III PI-3 kinase. *Mol Cancer Ther* **14**
53. Kabeya, Y., Mizushima, N., Ueno, T., Yamamoto, A., Kirisako, T., Noda, T., Kominami, E., Ohsumi, Y., and Yoshimori, T. (2000) LC3, a mammalian homologue of yeast Apg8p, is localized in autophagosome membranes after processing. *The EMBO journal* **19**, 5720-5728
54. Walczak, M., and Martens, S. (2013) Dissecting the role of the Atg12-Atg5-Atg16 complex during autophagosome formation. *Autophagy* **9**, 424-425
55. Peng, J., Zhang, R., Cui, Y., Liu, H., Zhao, X., Huang, L., Hu, M., Yuan, X., Ma, B., Ma, X., Takashi, U., Masaaki, K., Liang, X., and Yu, L. (2014) Atg5 regulates late endosome and lysosome biogenesis. *Sci China Life Sci* **57**, 59-68

56. Repnik, U., Cesen, M. H., and Turk, B. (2013) The endolysosomal system in cell death and survival. *Cold Spring Harbor perspectives in biology* **5**, a008755
57. Schwake, M., Schroder, B., and Saftig, P. (2013) Lysosomal membrane proteins and their central role in physiology. *Traffic* **14**, 739-748
58. Thoreen, C. C., Kang, S. A., Chang, J. W., Liu, Q., Zhang, J., Gao, Y., Reichling, L. J., Sim, T., Sabatini, D. M., and Gray, N. S. (2009) An ATP-competitive mammalian target of rapamycin inhibitor reveals rapamycin-resistant functions of mTORC1. *J Biol Chem* **284**, 8023-8032
59. Lauritzen, I., Pardossi-Piquard, R., Bauer, C., Brigham, E., Abraham, J. D., Ranaldi, S., Fraser, P., St-George-Hyslop, P., Le Thuc, O., Espin, V., Chami, L., Dunys, J., and Checler, F. (2012) The beta-secretase-derived C-terminal fragment of betaAPP, C99, but not Abeta, is a key contributor to early intraneuronal lesions in triple-transgenic mouse hippocampus. *J Neurosci* **32**, 16243-16255a
60. Billings, L. M., Oddo, S., Green, K. N., McGaugh, J. L., and LaFerla, F. M. (2005) Intraneuronal Abeta causes the onset of early Alzheimer's disease-related cognitive deficits in transgenic mice. *Neuron* **45**, 675-688
61. Lauritzen, I., Pardossi-Piquard, R., Bourgeois, A., Pagnotta, S., Biferi, M. G., Barkats, M., Lacor, P., Klein, W., Bauer, C., and Checler, F. (2016) Intraneuronal aggregation of the beta-CTF fragment of APP (C99) induces Abeta-independent lysosomal-autophagic pathology. *Acta Neuropathol*
62. Jiang, Y., Mullaney, K. A., Peterhoff, C. M., Che, S., Schmidt, S. D., Boyer-Boiteau, A., Ginsberg, S. D., Cataldo, A. M., Mathews, P. M., and Nixon, R. A. (2010) Alzheimer's-related endosome dysfunction in Down syndrome is Abeta-independent but requires APP and is reversed by BACE-1 inhibition. *Proc Natl Acad Sci U S A* **107**, 1630-1635
63. Bellettato, C. M., and Scarpa, M. (2010) Pathophysiology of neuropathic lysosomal storage disorders. *Journal of inherited metabolic disease* **33**, 347-362
64. Ohm, T. G., Treiber-Held, S., Distl, R., Glockner, F., Schonheit, B., Tamanai, M., and Meske, V. (2003) Cholesterol and tau protein--findings in Alzheimer's and Niemann Pick C's disease. *Pharmacopsychiatry* **36 Suppl 2**, S120-126
65. Rusten, T. E., and Stenmark, H. (2009) How do ESCRT proteins control autophagy? *J Cell Sci* **122**, 2179-2183
66. Lytton, J., Westlin, M., and Hanley, M. R. (1991) Thapsigargin inhibits the sarcoplasmic or endoplasmic reticulum Ca-ATPase family of calcium pumps. *J Biol Chem* **266**, 17067-17071
67. Xu, W., Weissmiller, A. M., White, J. A., Fang, F., Wang, X. Y., Wu, Y. W., Pearn, M. L., Zhao, X. B., Sawa, M., Chen, S. D., Gunawardena, S., Ding, J. Q., Mobley, W. C., and Wu, C. B. (2016) Amyloid precursor protein-mediated endocytic pathway disruption induces axonal dysfunction and neurodegeneration. *J Clin Invest* **126**, 1815-1833
68. Kim, S., Sato, Y., Mohan, P. S., Peterhoff, C., Pensalfini, A., Rigoglioso, A., Jiang, Y., and Nixon, R. A. (2016) Evidence that the rab5 effector APPL1 mediates APP-beta CTF-induced dysfunction of endosomes in Down syndrome and Alzheimer's disease. *Mol Psychiatr* **21**, 707-716
69. Jiang, Y., Rigoglioso, A., Peterhoff, C. M., Pawlik, M., Sato, Y., Bleiwas, C., Stavrides, P., Smiley, J. F., Ginsberg, S. D., Mathews, P. M., Levy, E., and Nixon, R. A. (2016) Partial BACE1 reduction in a Down syndrome mouse model blocks Alzheimer-related endosomal anomalies and cholinergic neurodegeneration: role of APP-CTF. *Neurobiology of Aging* **39**, 90-98
70. Razi, M., Chan, E. Y. W., and Tooze, S. A. (2009) Early endosomes and endosomal coatomer are required for autophagy. *Journal of Cell Biology* **185**, 305-321
71. Berg, T. O., Fengsrud, M., Stromhaug, P. E., Berg, T., and Seglen, P. O. (1998) Isolation and characterization of rat liver amphisomes - Evidence for fusion of autophagosomes with both early and late endosomes. *Journal of Biological Chemistry* **273**, 21883-21892
72. Koo, E. H., and Squazzo, S. L. (1994) Evidence that production and release of amyloid beta-protein involves the endocytic pathway. *J Biol Chem* **269**, 17386-17389
73. Xu, H., Sweeney, D., Wang, R., Thinakaran, G., Lo, A. C., Sisodia, S. S., Greengard, P., and Gandy, S. (1997) Generation of Alzheimer beta-amyloid protein in the trans-Golgi network in the apparent absence of vesicle formation. *Proc Natl Acad Sci U S A* **94**, 3748-3752

74. Spilman, P., Podlutskaya, N., Hart, M. J., Debnath, J., Gorostiza, O., Bredesen, D., Richardson, A., Strong, R., and Galvan, V. (2010) Inhibition of mTOR by rapamycin abolishes cognitive deficits and reduces amyloid-beta levels in a mouse model of Alzheimer's disease. *PLoS One* **5**, e9979

75. Harrison, D. E., Strong, R., Sharp, Z. D., Nelson, J. F., Astle, C. M., Flurkey, K., Nadon, N. L., Wilkinson, J. E., Frenkel, K., Carter, C. S., Pahor, M., Javors, M. A., Fernandez, E., and Miller, R. A. (2009) Rapamycin fed late in life extends lifespan in genetically heterogeneous mice. *Nature* **460**, 392-395

FIGURE LEGENDS

Figure 1. Lysosomal activity inhibition increases APP-GFP and C99-GFP levels. (A) Schematic representation of APP proteolytic processing indicating the N-terminal (*N*) luminal domain (*Luminal/Extracellular*), transmembrane domain (*TM*), C-terminal (*C*) cytosolic domain (*Cytosolic*), with the position of the α, β and γ cleavage sites, the resulting C-terminal fragments C99, C83, and AICDγ, and the Aβ and p3 peptides. Lines depict APP regions recognized by the antibodies used in this study (*WO2* and *Anti-Tail*). The inhibitory effect of DAPT on γ-secretase activity and the localization of the green fluorescent protein (*GFP*) moiety are also indicated. **(B)** H4 cells stably expressing an amyloidogenic version of GFP-tagged APP were left untreated (lane 1) or treated either with 1 μM DAPT for 16 h (lane 2), 200 μM chloroquine (*CQ*) for 4 h (lane 3), 1 μM DAPT for 12 h followed by a combination of 1 μM DAPT and 200 μM CQ for 4 h (lane 4), 100 nM bafilomycin A1 (*BfaA1*) for 4 h (lane 5), or 1 μM DAPT for 12 h followed by a combination of 1 μM DAPT and 100 nM BfaA1 for 4 h (lane 6). Detergent-soluble protein extracts were analyzed by western blot either with anti-GFP (to detect GFP-tagged APP, C83 and AICDγ), the monoclonal antibody WO2 (used to show the detection of only C99-GFP), or with anti-β-actin used as a loading control. The position of molecular mass markers is indicated on the left. **(C)** Densitometric quantification of the western blot signal of GFP-tagged APP (*APP-GFP*), C99 (*C99-GFP*) and C83 (*C83-GFP*) from cells treated with DAPT alone (*Control*), or in combination with either CQ or BfaA1, as shown in A. Bars represent the mean ± standard deviation of the western blot signal normalized with the β-actin signal (n=3). * $P < 0.05$, ** $P < 0.01$ and *** $P < 0.001$.

Figure 2. TSG101 depletion increases the levels of APP species generated from an amyloidogenic version of APP-GFP. (A) H4 cells stably expressing an amyloidogenic version of GFP-tagged APP were transfected with either a control siRNA (*siNT*) or a siRNA targeting TSG101 (*siTSG101*), and further left untreated (lanes 1 and 3), or treated with 1 μM DAPT for 16 h (lanes 2 and 4). Detergent-soluble protein extracts were analyzed by western blot either with anti-GFP (to detect GFP-tagged APP, C99, C83 and AICDγ), the monoclonal antibody WO2 (used to show the detection of only C99-GFP; *C99-GFP**), or anti-TSG101. Western blot with anti-β-actin was used as a loading control. The position of molecular mass markers is indicated on the left. **(B)** Densitometric quantification of the western blot signal of GFP-tagged APP (*APP-GFP*), C99 (*C99-GFP*) and C83 (*C83-GFP*) in cells treated with DAPT, as shown in (A). Bars represent the mean ± standard deviation of the western blot signal normalized with the β-actin signal (n=3). ** $P < 0.01$ and *** $P < 0.001$.

Figure 3. Selective inhibition of the class III phosphatidylinositol 3-kinase Vps34 inhibits basal autophagy and autophagy induced by nutrient starvation, and increases the levels of endogenous C99. H4 cells were left untreated **(A-C)**, or treated either with Earle's balanced salt solution (*EBSS*) for 1 h **(D-F)**, 1 μM Vps34-IN1 for 1 h **(G-I)**, or a combination of 1 μM Vps34-IN1 and EBSS for 1 h **(J-L)**. Cells were fixed, permeabilized, and incubated with anti-LC3 (A, D, G and J) and with anti-p62 (B, E, H and K), followed by incubation with Alexa-488-conjugated donkey anti-rabbit IgG (green channels) and Alexa-594-conjugated donkey anti-mouse IgG (red channels). Images were acquired by fluorescence microscopy. Merging green and red channels generated the third image in each row; yellow indicates overlapping of the green and red channels. Bar, 10 μm. **(M)** Quantification of the number of LC3- or p62-containing puncta per cell in response to incubation with EBSS for 1 h or a combination of 1 μM Vps34-IN1 and EBSS for 1 h. Bars represent the mean ± standard deviation (n=10). **(N)** H4 cells were treated either with 2 μM DAPT (*Control*) for 16 h (lane 1), with 2 μM DAPT for 15 h followed by a combination of 2 μM DAPT and 1 μM Vps34-IN1 for 1 h (lane 2), or with 2 μM DAPT for 14 h followed by a combination of 2 μM DAPT and 1 μM Vps34-IN1 for 2 h (lane 3). Detergent-soluble protein extracts were analyzed by western blot with either an antibody targeting the cytosolic tail of APP (to detect APP and C83), the monoclonal antibody WO2 (used to show the detection of only C99), or an anti-LC3 antibody that detects both LC3-I and LC3-II. Western blot with anti-β-actin was used as a loading control. The position of molecular mass markers is indicated on the left.

Figure 4. Atg5 depletion accumulates C99 and C83. (A) H4 cells stably expressing a control shRNA (*shLuc*) or a shRNA targeting Atg5 (*shAtg5*) were left untreated (-) or treated (+) with 2 μM DAPT for 16 h. Detergent-soluble protein extracts were analyzed by western blot with either an antibody targeting the cytosolic tail of APP (to detect APP and C83), the monoclonal antibody WO2 (used to show the detection of only C99), or an anti-Atg5 antibody that detects the Atg5-Atg12 conjugate. Western blot with anti-β-actin was used as a loading control. The position of molecular mass markers is indicated on the left. **(B)** Densitometric quantification of APP, C99 and C83 western blot signals in cells treated without DAPT, as shown in (A). **(C)** Densitometric quantification of APP, C99 and C83 western blot signals in cells treated with DAPT, as shown in (A). **(D)** Densitometric quantification of C99 and C83 western blot signals in Atg5 depleted cells (*shAtg5*) that were left untreated (-) or treated with DAPT (+), as shown in (A). Bars represent the mean ± standard deviation of the western blot signal normalized with the β-actin signal (n=3). * $P < 0.05$, ** $P < 0.01$.

Figure 5. Atg5 depletion increases the amount of endogenous APP and CTFs localized in an enlarged LAMP1-containing endo-lysosomal compartment. (A-H) H4 cells stably expressing either a control shRNA (*shLuc*, A-D) or a shRNA targeting Atg5 (*shAtg5*, E-H) were fixed, permeabilized, and incubated with an

antibody targeting the cytosolic tail of APP (to detect APP, C99, C83 and AICDγ; *APP/CTFs*; A and E), with anti-LAMP1 (B and F), and with anti-EEA1 (C and G), followed by Alexa-488-conjugated donkey anti-rabbit IgG (green channels), Alexa-594-conjugated donkey anti-mouse IgG (red channels) and Alexa-647-conjugated goat anti-human IgG (blue channels). Images were acquired by laser scanning confocal microscopy. Merging green, red and blue channels generated the fourth image in each row; yellow indicates overlapping of the green and red channels, cyan indicates overlapping of the green and blue channels, magenta indicates overlapping of the red and blue channels, and white indicates overlapping of all channels. Insets show 3x magnifications with arrows indicating colocalization of APP/CTFs and EEA1 in shLuc cells or colocalization of APP/CTFs and LAMP1 in shAtg5 cells. Bar, 10 μm. **(I)** Quantification of the fluorescence signal of APP/CTFs that colocalized with the fluorescence signal of LAMP1, from images as shown in A and B of control cells (*shLuc*), or as shown in E and F of Atg5 depleted cells. **(J)** Quantification of the fluorescence signal of APP/CTFs that colocalized with the fluorescence signal of EEA1, from images as shown in A and C of control cells (*shLuc*), or as shown in E and G of Atg5 depleted cells. Bars represent the mean ± standard deviation (n=12). **(K and L)** Scatter plot graphs with Pearson's correlation coefficients obtained from the colocalization analysis shown in I and J. **(M)** Quantification of the fluorescence intensity of APP species shown in A and E. Bars represent the mean ± standard deviation of the fluorescent signal per cell area (n=12). *** $P \leq 0.001$.

Figure 6. Super resolution microscopy revealed that Atg5 depletion accumulates APP/CTFs in the lumen of enlarged LAMP1-containing endo-lysosomal compartments. (A-G) H4 cells stably expressing either control shRNA (*shLuc*, A-C) or a shRNA targeting Atg5 (*shAtg5*, D-G) were fixed, permeabilized, and incubated with an antibody targeting the cytosolic tail of APP (to detect APP, C99, C83 and AICDγ; *APP/CTFs*; A, D and G) and anti-LAMP1 (B, E and G), followed by Alexa-488-conjugated donkey anti-rabbit IgG (green channels) and Alexa-594-conjugated donkey anti-mouse IgG (red channels). Nuclei were stained with DAPI (blue channels). Images were acquired by structured illumination microscopy. Merging green, red and blue channels generated the third image in the first two rows. The image shown in G is a composite of the green and red channels of a threefold magnified region representative of an image similar to that shown in F. Bars: A-F, 1 μm; G, 200 nm. **(H)** Graph representing a scan of the fluorescence signal of APP/CTFs and LAMP1 along the dashed line shown in (G).

Figure 7. Activation of autophagy by nutrient starvation and Torin-1 treatments decreases C99 levels. (A and C) H4 cells stably expressing an amyloidogenic version of GFP-tagged C99 were incubated with Earl's Salt Balance Solution (*EBSS*; A), or with 250 nM Torin-1 (C), for the indicated periods of time. Detergent-soluble protein extracts were analyzed by western blot with anti-GFP (to detect GFP-tagged C99 and AICDγ). Western blot with anti-β-actin was used as a loading control. The position of molecular mass markers is indicated on the

left. **(B and D)** Densitometric quantification of C99-GFP and AICDγ-GFP western blot signals, at time = 0 (*Control*) and after 4 h of treatment either with EBSS (B) (as shown in A), or with Torin-1 (D) (as shown in C). Bars represent the mean ± standard deviation of the western blot signal normalized with the β-actin signal (n=3). **(E)** Alternatively, cells were left untreated (lane 1), or treated with 2 μM DAPT for 16 h (lanes 2, 3 and 5), or treated with 2 μM DAPT for 12 h followed by either a combination of 2 μM DAPT and EBSS for 4 h (lane 4), or a combination of 2 μM DAPT and 250 nM Torin-1 for 4 h (lane 6). **(F)** Densitometric quantification of the C99-GFP western blot signal in cells treated with DAPT alone (*Control*), or in combination with either EBSS or Torin-1, as shown in (E). Bars represent the mean ± standard deviation of the amount of western blot signal normalized with the β-actin signal (n=3). ** $P < 0.01$.

Figure 8. Model of the mechanism underlying the turnover of APP and CTFs via Atg5-dependent macroautophagy. APP, C99 and C83 can reach an early endosome either (*1*) via the *trans*-Golgi network (*TGN*), or (*2*) via the cell surface. (*3*) An early endosome matures to a late endosome, also called a multivesicular body (*MVB*). (*4*) APP, C99 and C83 are incorporated into intraluminal vesicles of an MBV in a process facilitated by the ESCRT machinery (*ESCRT-0 - ESCRT-III*), in which TSG101 is part of ESCRT-I. (*5*) In parallel, the Atg5-Atg12-Atg16L complex facilitates LC3 lipidation (*LC3-I*) with phosphatidylethanolamine. (*6*) Lipidated LC3 (*LC3-II*) associates to a pre-autophagosomal membrane called a phagophore, a process that promotes recruitment of autophagy cargos and adaptor proteins, such as p62. (*7*) The phagophore matures to form an autophagosome, a double-membrane-bound organelle. (*8*) An autophagosome can fuse with endo-lysosomal compartments, such as a MVB. The fusion of an autophagosome with a MVB results in the formation of a hybrid organelle called amphisome. (*9*) An amphisome can fuse with a lysosome promoting the final degradation of APP, C99 and C83.

Figure S1. Lysosomal activity inhibition increases the levels of endogenous C99. H4 cells were left untreated (lane 1), or treated either for 4 h with a cocktail of lysosomal inhibitors composed of 100 nM bafilomycin A1 (*BfaA1*), 10 μM E64D, and 70 μg/ml leupeptin (lane 2), or for 16 h with 2 μM DAPT (lane 3), or for 12 h with 2 μM DAPT followed by 4 h with a combination of 2 μM DAPT and the cocktail of lysosomal inhibitors (lane 4). Detergent-soluble protein extracts were analyzed by western blot with the monoclonal antibody WO2. Western blot with anti-β-actin was used as a loading control. The position of molecular mass markers is indicated on the left.

Figure S2. TSG101 depletion produces APP-GFP accumulation in enlarged LAMP1-containing endo-lysosomal compartments. (A-F) H4 cells stably expressing an amyloidogenic version of GFP-tagged APP

(green channel) were transfected with either a control siRNA (*siNT*; A-C) or a siRNA targeting TSG101 (*siTSG101*; D-F). After 48 h, cells were fixed, permeabilized, and incubated with anti-LAMP1, followed by incubation with Alexa-594-conjugated donkey anti-mouse IgG (red channel). Images were acquired by laser scanning confocal microscopy. Merging green and red channels generated the third image in each row; yellow indicates overlapping of the green and red channels. Bar, 10 μm. **(G)** Quantification of the fluorescence signal of APP-GFP species that colocalized with the fluorescence signal of LAMP1, from images as shown in A-E. Bars represent the mean ± standard deviation (n=12). **(H)** Scatter plot graph with Pearson's correlation coefficients obtained from the colocalization analysis shown in (G). *** $P < 0.001$.

Figure S3. TSG101 depletion produces accumulation of p62- and LC3-containing puncta. (A-M) H4 cells were transfected with either a control siRNA (*siNT*; A-C and H-J) or a siRNA targeting TSG101 (*siTSG101*; D-F and K-M). After 72 h, cells were fixed, permeabilized, and co-incubated either with anti-p62 (A and D) and anti-LC3 (B and E), or with anti-p62 (H and K) and anti-Cathepsin D (I and L), followed by Alexa-594-conjugated donkey anti-mouse IgG (red channels) and Alexa-488-conjugated donkey anti-mouse IgG (green channels). Nuclei were stained with DAPI (blue channels). Images were acquired by laser scanning confocal microscopy. Merging red, green and blue channels generated the third image in each row. Bars, 10 μm. **(G)** Quantification of the number of p62-containing puncta per cell. Bars represent the mean ± standard deviation (n=10). **(N)** Colocalization analysis of images from cells transfected with the siRNA targeting TSG101. The graph depicts the quantification of the fluorescence signal of either LC3 or Cathepsin D (*Cat D*) that colocalized with the fluorescence signal of p62, from images as shown in D and E, and K and L, respectively. Bars represent the mean ± standard deviation (n=12). *** $P < 0.001$.

Figure S4. Thapsigargin treatment produces accumulation of p62- and LC3-containing autophagosomes, and increases the levels of GFP-tagged APP species. (A-H) H4 cells were left untreated or treated with 2 μM thapsigargin for 16 h. Cells were fixed, permeabilized, and incubated with antibodies targeting p62 (A and E), LC3 (B and F) or Cathepsin D (C and G), followed by Alexa-594-conjugated donkey anti-mouse IgG (red channels), Alexa-488-conjugated donkey anti-rabbit IgG (green channels), and Alexa-647-conjugated donkey anti-goat IgG (blue channels). Images were acquired by epifluorescence microscopy. Merging green, red and blue channels generated the fourth image in each row; yellow indicates overlapping of the green and red channels. Bar, 10 μm. **(I and J)** Colocalization analysis of images from cells treated with thapsigargin. In I the graph depicts the quantification of the fluorescence signal of p62 that colocalized with the fluorescence signal of either LC3 or Cathepsin D, from images as shown in E and F, or in E and G, respectively, and the quantification of the fluorescence signal of LC3 that colocalized with the fluorescence signal of Cathepsin D, from images as shown in F and G. Bars represent the mean ± standard deviation (n=12). In J the graph depicts a

scatter plot with Pearson's correlation coefficients obtained from the colocalization analysis shown in I. *** $P < 0.001$. **(K)** H4 cells stably expressing an amyloidogenic version of GFP-tagged APP were treated with 2 μM DAPT for 16 h (lane 1) or with a combination of 2 μM DAPT and 2 μM thapsigargin for 16 h (lane 2). Detergent-soluble protein extracts were analyzed by western blot either with anti-GFP (to detect GFP-tagged APP and C83), the monoclonal antibody WO2 (used to show the detection of only C99-GFP), or anti-β-actin (used as loading control). The position of molecular mass markers is indicated on the left. **(L)** Densitometric quantification of the western blot signal of GFP-tagged APP species, as shown in K. Bars represent the mean ± standard deviation of the amount of immunoblot signal normalized with the β-actin signal (n=3). ** $P < 0.01$; *n.s.*, not statistically significant.

Figure S5. Reduced endogenous APP levels in cells depleted of Atg5 are not rescued by inhibitors of lysosomal degradation. H4 cells stably expressing a control shRNA (*shLuc*) or a shRNA targeting Atg5 (*shAtg5*) were left untreated (lanes 1 and 4) or treated 4 or 8 hours (*h*) with a cocktail of lysosomal inhibitors composed of 50 nM bafilomycin A1 (*BfaA1*), 10 μM E64D, and 70 μg/ml leupeptin. Detergent-soluble protein extracts were analyzed by western blot with an antibody targeting the cytosolic tail of APP. Western blot with anti-β-actin was used as a loading control. The position of molecular mass markers is indicated on the left.

Figure S6. Atg5 depletion increases the amount of endogenous APP and CTFs localized in an enlarged endo-lysosomal compartment containing LAMP1 and Cathepsin D. (A-H) H4 cells stably expressing either a control shRNA (*shLuc*, A-D) or a shRNA targeting Atg5 (*shAtg5*, E-H) were fixed, permeabilized, and incubated with antibodies targeting either the cytosolic tail of APP (to detect APP, C99, C83 and AICDγ; *APP/CTFs*; A and E), LAMP1 (B and F) or Cathepsin D, followed by Alexa-488-conjugated donkey anti-rabbit IgG (green channels), Alexa-594-conjugated donkey anti-mouse IgG (red channels) and Alexa-647-conjugated donkey anti-goat IgG (blue channels). Images were acquired by laser scanning confocal microscopy. Merging green, red and blue channels generated the fourth image in each row; white indicates overlapping of the green, red and blue channels. Bar, 10 μm. **(I)** Quantification of the fluorescence signal of APP/CTFs that colocalized with the fluorescence signal of LAMP1, from images as shown in A and B of control cells (*shLuc*), or as shown in E and F of Atg5 depleted cells. **(J)** Quantification of the fluorescence signal of APP/CTFs that colocalized with the fluorescence signal of Cathepsin D, from images as shown in A and C of control cells (*shLuc*), or as shown in E and G of Atg5 depleted cells. **(K)** Quantification of the fluorescence signal of Cathepsin D (*CatD*) that colocalized with the fluorescence signal of LAMP1, from images as shown in B and C of control cells (*shLuc*), or as shown in F and G of Atg5 depleted cells. Bars represent the mean ± standard deviation (n=12). **(L**

and M) Scatter plot graphs with Pearson's correlation coefficients obtained from the colocalization analysis shown in J and K.

Figure S7. Atg5 depletion caused the appearance of perinuclear enlarged organelles decorated with antibody to Cathepsin D, CD63 and LAMP2. (A-L) H4 cells stably expressing either a control shRNA (*shLuc*, A-C and G-I) or a shRNA targeting Atg5 (*shAtg5*, D-F and J-L) were fixed, permeabilized, and incubated with antibodies targeting either Cathepsin D (A, D, G and J), CD63 (B and E), or LAMP2 (H and K), followed by Alexa-488-conjugated donkey anti-goat IgG (green channels), and Alexa-594-conjugated donkey anti-mouse IgG (red channels). Images were acquired by laser scanning confocal microscopy. Merging green and red channels generated the third image in each row; yellow indicates overlapping of the green and red channels. Bar, 10 μm. **(M)** Quantification of the fluorescence signal of Cathepsin D that colocalized with the fluorescence signal of CD63, from images as shown in A and B of control cells (*shLuc*), or as shown in D and E of Atg5 depleted cells. **(N)** Quantification of the fluorescence signal of Cathepsin D that colocalized with the fluorescence signal of LAMP2, from images as shown in G and H of control cells (*shLuc*), or as shown in J and K of Atg5 depleted cells. Bars represent the mean ± standard deviation (n=12). **(O and P)** Scatter plot graphs with Pearson's correlation coefficients obtained from the colocalization analysis shown in M and N.

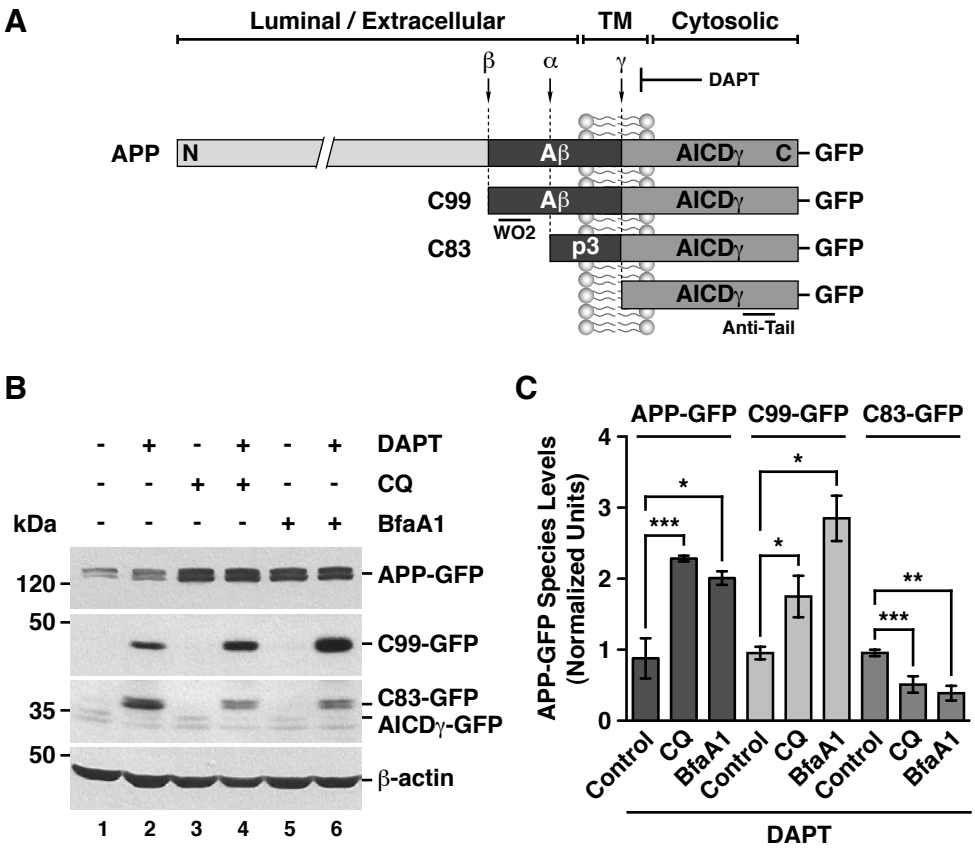

Figure 1
González et al., 2016

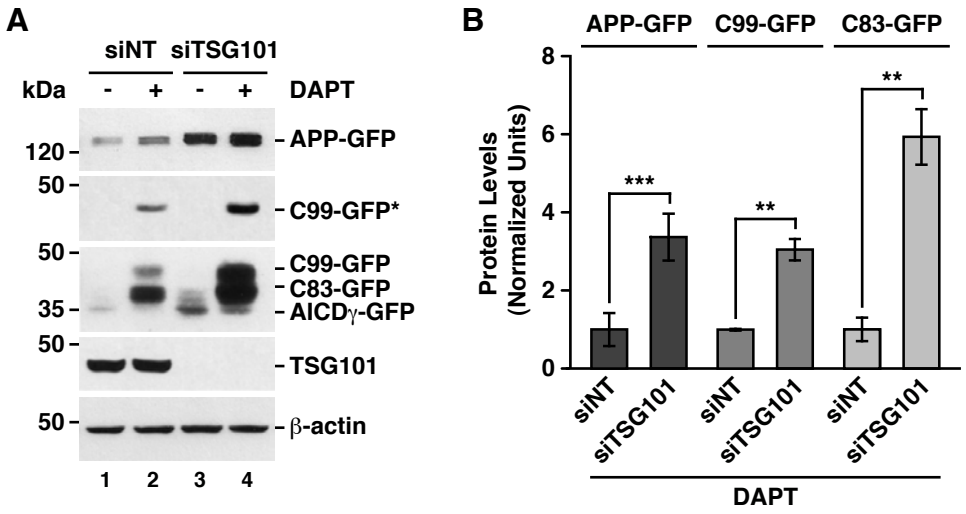

Figure 2
González et al., 2016

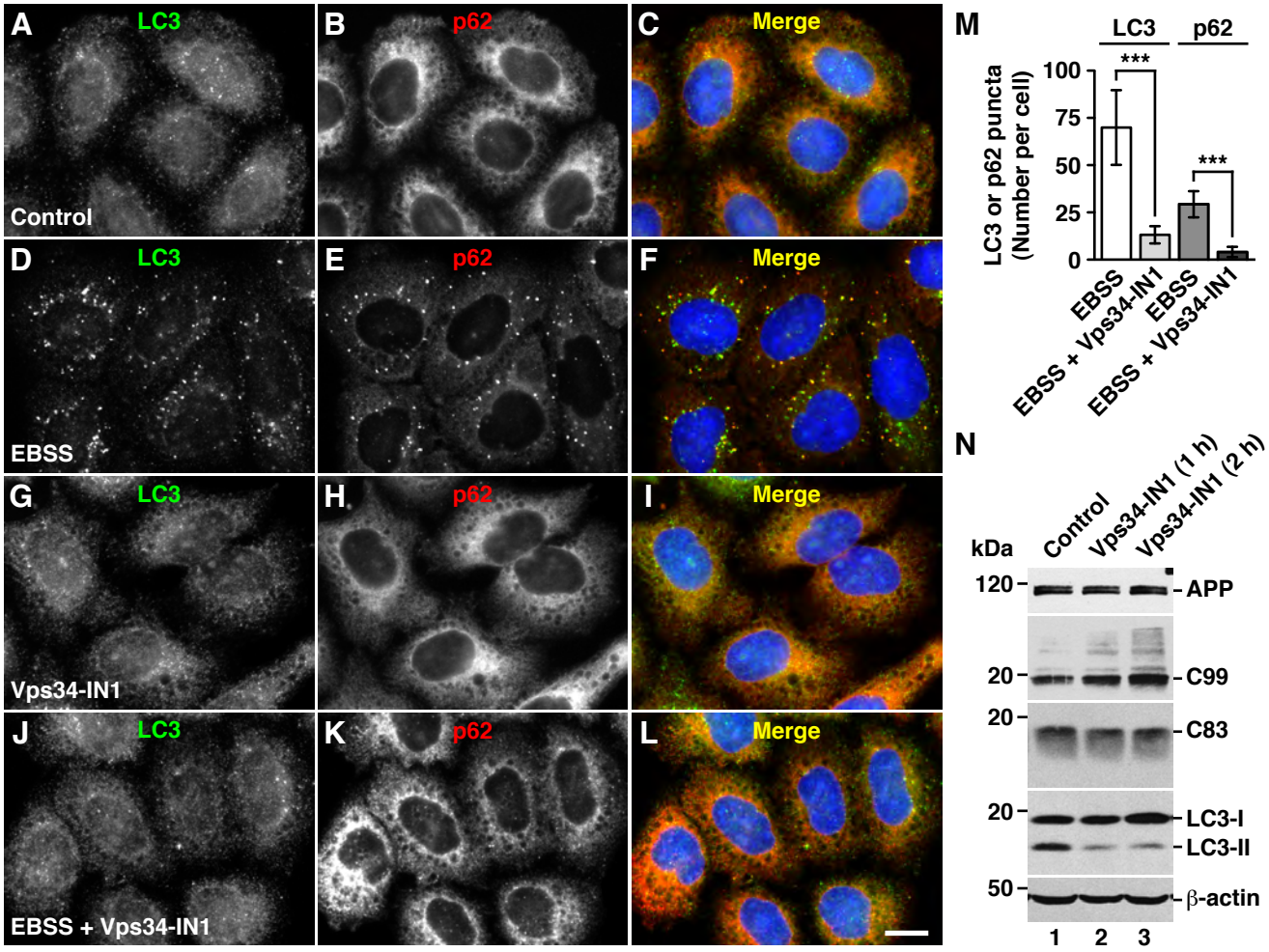

Figure 3
González et al., 2016

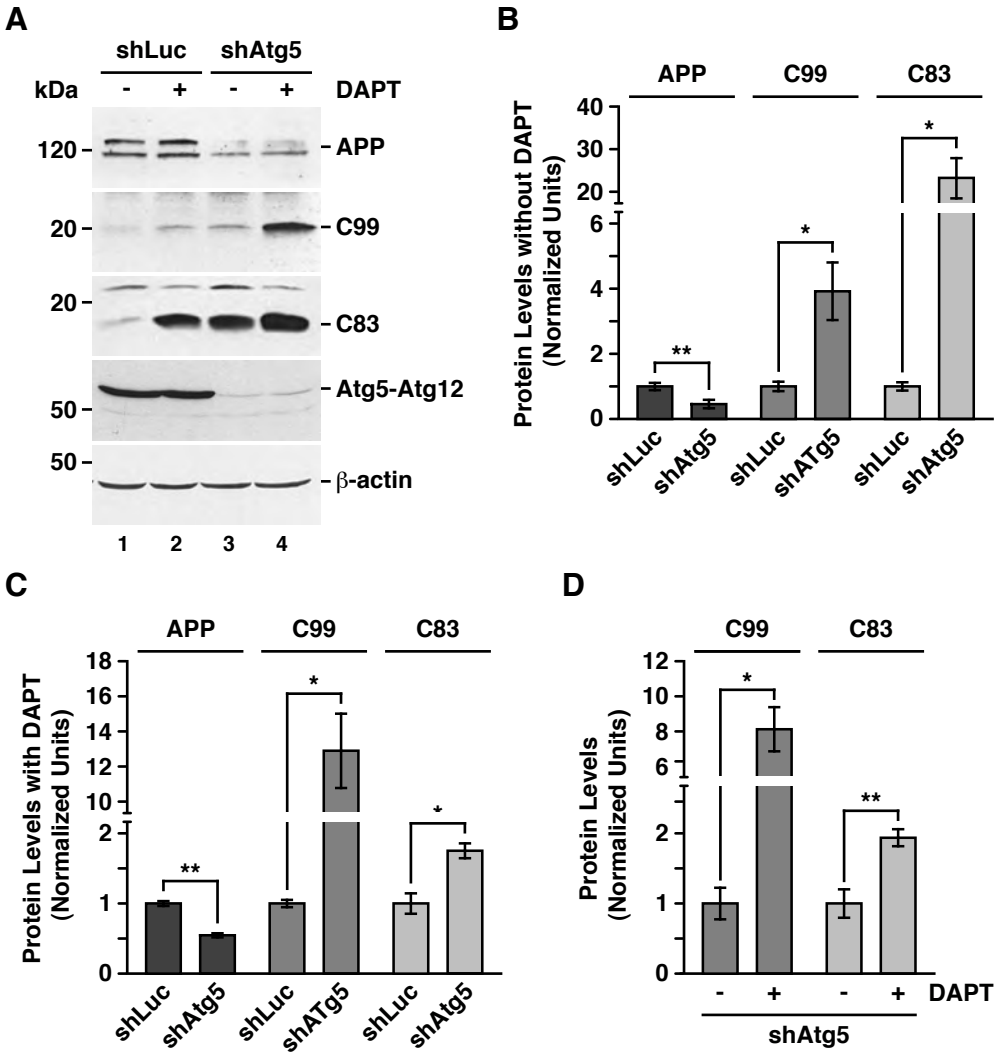

Figure 4
González et al., 2016

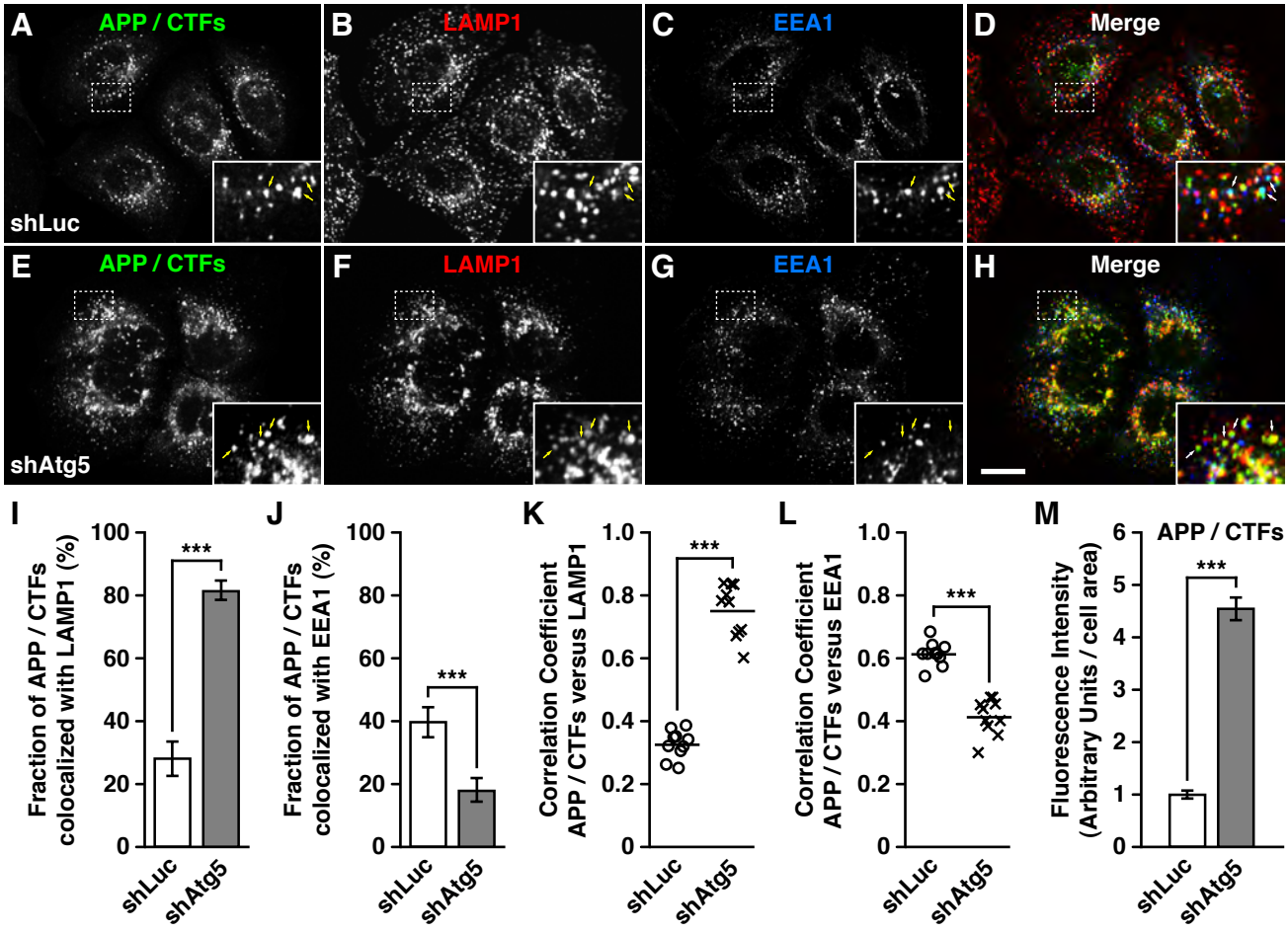

Figure 5
González et al., 2016

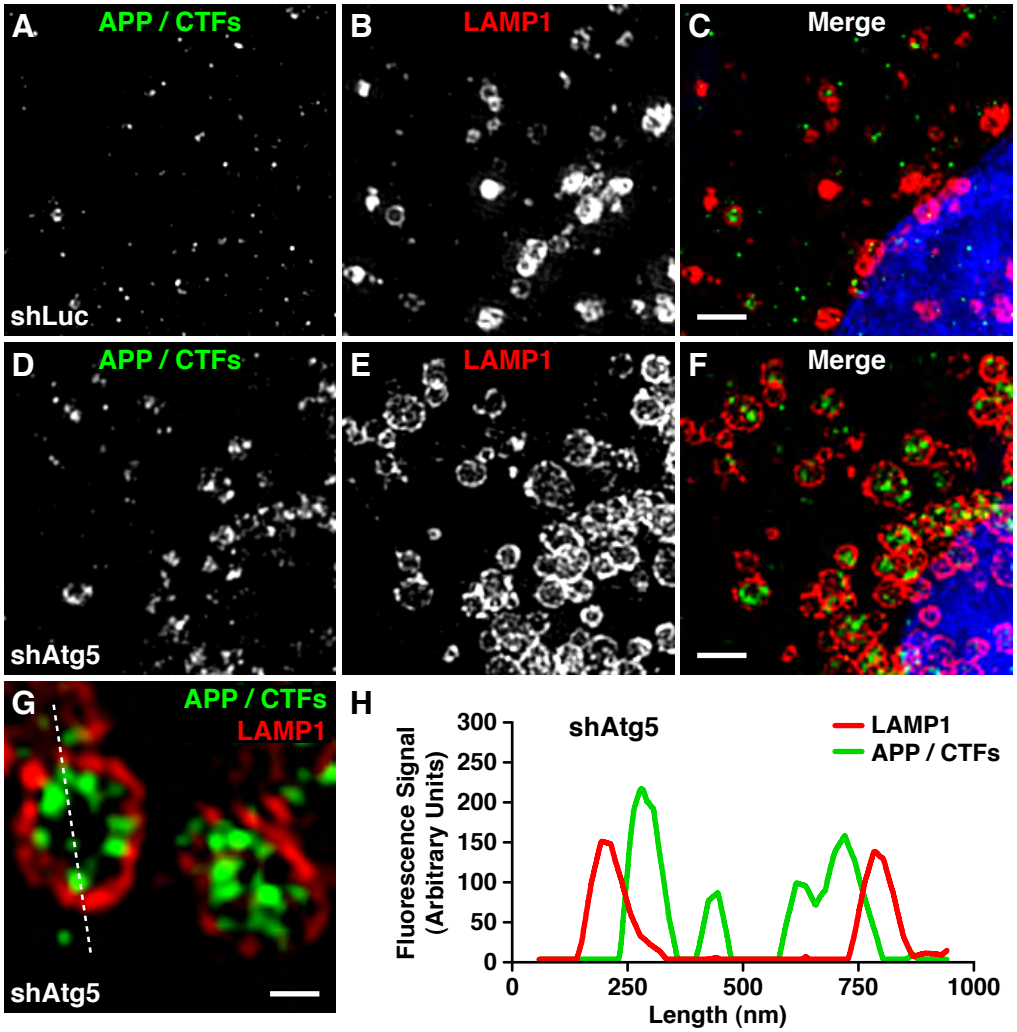

Figure 6
González et al., 2016

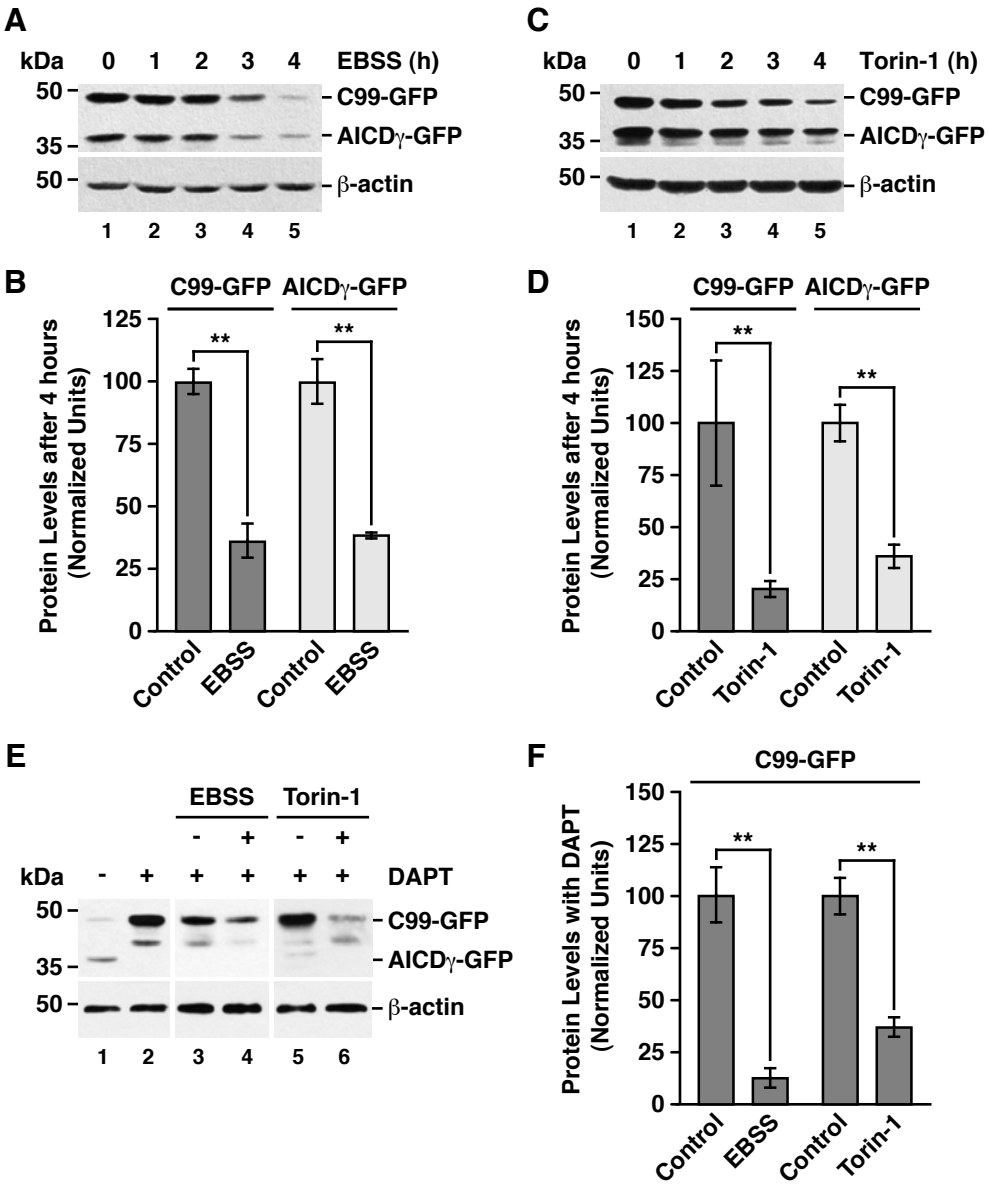

Figure 7
González et al., 2016

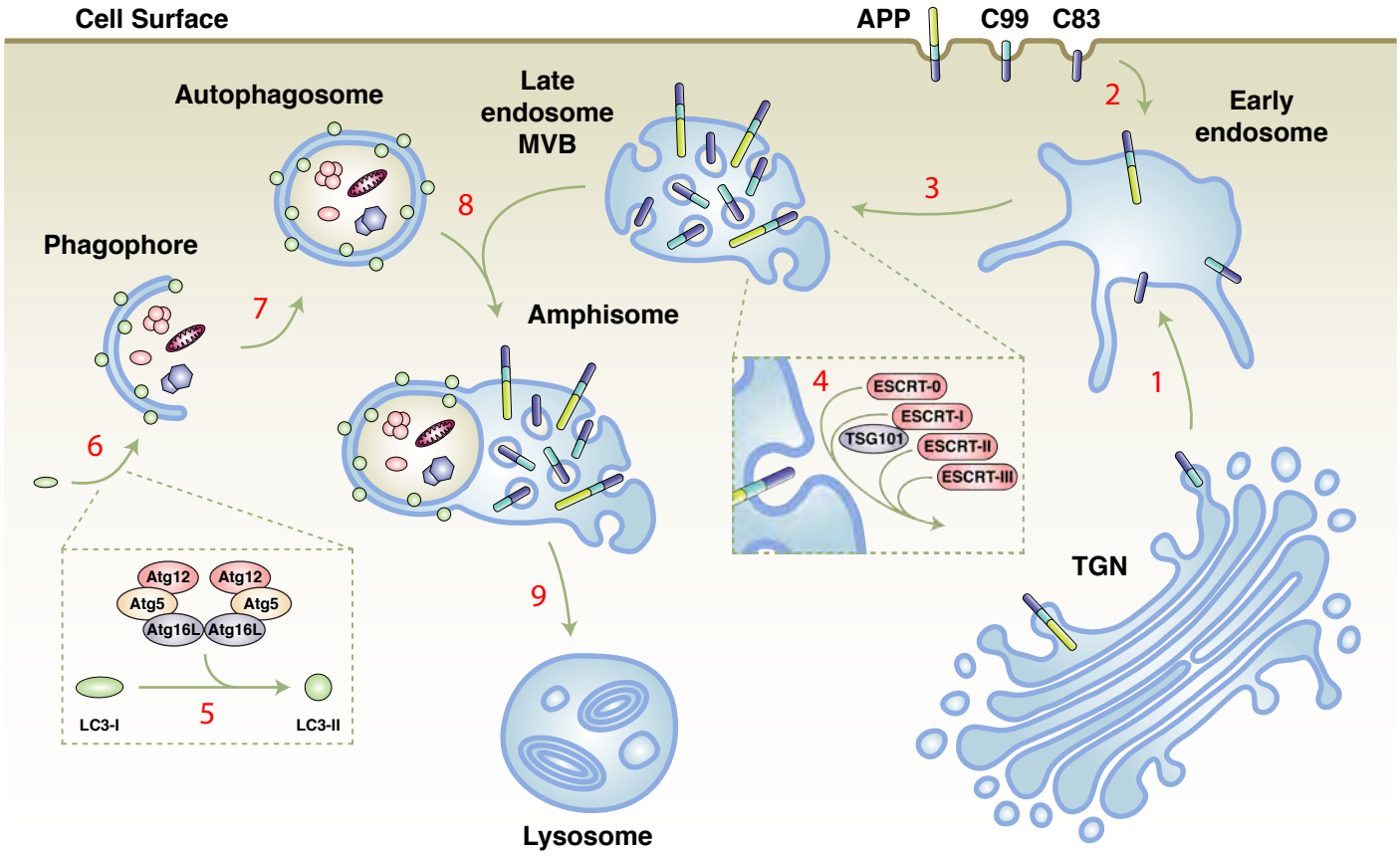

Figure 8
González et al., 2016